Talin-bound NPLY motif recruits integrin-signaling adapters to regulate cell spreading and mechanosensing

Perrine Pinon,[1] Jenita Pärssinen,[2,3] Patricia Vazquez,[1] Michael Bachmann,[4] Rolle Rahikainen,[2,3] Marie-Claude Jacquier,[1] Latifeh Azizi,[2,3] Juha A. Määttä,[2,3] Martin Bastmeyer,[4,5] Vesa P. Hytönen,[2,3] and Bernhard Wehrle-Haller[1]

[1]Department of Cell Physiology and Metabolism, University Medical Center, University of Geneva, 1211 Geneva, Switzerland
[2]BioMediTech, University of Tampere, 33520 Tampere, Finland
[3]Fimlab Laboratories, 33520 Tampere, Finland
[4]Institute of Zoology and [5]Institute of Functional Interfaces, Karlsruhe Institute of Technology, 76131 Karlsruhe, Germany

Integrin-dependent cell adhesion and spreading are critical for morphogenesis, tissue regeneration, and immune defense but also tumor growth. However, the mechanisms that induce integrin-mediated cell spreading and provide mechanosensing on different extracellular matrix conditions are not fully understood. By expressing β3-GFP-integrins with enhanced talin-binding affinity, we experimentally uncoupled integrin activation, clustering, and substrate binding from its function in cell spreading. Mutational analysis revealed Tyr747, located in the first cytoplasmic NPLY^{747} motif, to induce spreading and paxillin adapter recruitment to substrate- and talin-bound integrins. In addition, integrin-mediated spreading, but not focal adhesion localization, was affected by mutating adjacent sequence motifs known to be involved in kindlin binding. On soft, spreading-repellent fibronectin substrates, high-affinity talin-binding integrins formed adhesions, but normal spreading was only possible with integrins competent to recruit the signaling adapter protein paxillin. This proposes that integrin-dependent cell–matrix adhesion and cell spreading are independently controlled, offering new therapeutic strategies to modify cell behavior in normal and pathological conditions.

Introduction

Heterodimeric receptors of the integrin family are critical to maintain the mechanical link between the ECM and the cytoskeleton. ECM-bound integrins induce also intracellular signaling, mediating cell spreading, migration, proliferation, and survival (Akiyama et al., 1994; Hynes, 2002; Green et al., 2009). Importantly, both the anchoring and signaling function of integrins are required for controlling tissue morphogenesis, causing for example tumor formation and metastasis when misregulated (Paszek et al., 2005). To treat these pathologies, it is critical to understand the adhesion-mediating cytoskeleton–integrin–matrix connection but also to reveal the mechanisms leading to integrin-mediated signaling, which is also termed mechanosensing.

Integrin signaling is for example manifested by the local activation of the Rac1 GTPase, which causes the formation of lamellipodia and cell spreading, at sites where exploring filopodia contact immobilized integrin ligands (Guillou et al., 2008). At the filopodia/ECM interface, the clustering of integrins, which reflects an increase in integrin concentration and nascent adhesion formation, correlates with the accumulation of the cytoplasmic adapter protein talin and subsequent recruitment of paxillin and FAK (Partridge and Marcantonio, 2006). Although talin assures the mechanical link between the integrin and the actin cytoskeleton (Wehrle-Haller, 2012), the recruitment of paxillin and FAK to nascent adhesions (Choi et al., 2011) regulates cell spreading and mechanosensing (Hagel et al., 2002; Wade et al., 2002; Friedland et al., 2009; Choi et al., 2013). However, talin appears to play a dual role because its knockout or knockdown

J. Pärssinen, P. Vazquez, M. Bachmann, and R. Rahikainen contributed equally to this paper.

Correspondence to Bernhard Wehrle-Haller: Bernhard.Wehrle-Haller@unige.ch

Abbreviations used in this paper: CMA, cell–matrix adhesion; FN, fibronectin; HSA, human serum albumin; NHS, *N*-hydroxysuccinimide; NMR, nuclear magnetic resonance; NTA, nitrilotriacetic acid; PAA, polyacrylamide; PI(4,5)P_2, phosphatidylinositol 4,5-biphosphate; PTB, phosphotyrosine binding; SIM, structured illumination microscopy; TIRF, total internal reflection fluorescence; VN, vitronectin.

The Rockefeller University Press $30.00
J. Cell Biol. Vol. 205 No. 2 265–281
www.jcb.org/cgi/doi/10.1083/jcb.201308136

affected cell spreading and mechanosensing (Petrich et al., 2007b; Zhang et al., 2008; Monkley et al., 2011), which correlated with a failure to recruit paxillin and phospho-FAK, proposing a role of talin in the recruitment of these signaling adapters (Zhang et al., 2008). Indeed, talin is a key player in controlling integrin activation and the mechanical coupling of integrins to ECM ligands. To keep the integrin in an activated state, the talin head interacts with the membrane-proximal and the W/NPLY motif in the β integrin cytoplasmic tail (Tadokoro et al., 2003; Wegener et al., 2007) as well as phosphatidylinositol 4,5-biphosphate ($PI(4,5)P_2$) membrane lipids that open up the closed talin conformation and stabilize talin head–β integrin tail association (Goksoy et al., 2008; Saltel et al., 2009; Song et al., 2012). This results in α/β integrin tail unclasping, which leads to increased ligand binding in the integrin ectodomain, in a process called inside-out activation (Anthis et al., 2009). In turn, ECM ligands stabilize the conformational rearrangements in the integrin ectodomain in a process called outside-in activation (Zhu et al., 2013), which reinforces the ligand- and talin-bound integrin conformation (Wehrle-Haller, 2012). In addition, talin plays an important role in enhancing integrin binding to multivalent ligands by inducing integrin clustering (Bunch, 2010). Integrin clustering requires the activated integrin conformation and the $PI(4,5)P_2$-dependent interaction of the talin head with the membrane-proximal integrin tail (Cluzel et al., 2005; Saltel et al., 2009). Despite the critical role of talin in integrin activation and clustering, it is still not known whether talin is just keeping the integrin in a ligand-bound and signaling-competent state or whether it forms an essential part of the cytoplasmic scaffold required for recruitment of signaling adapters.

To answer this critical question, the integrin–talin association needs to be analyzed in the context of integrin signaling. As a convenient readout of integrin signaling, ligand-induced cell spreading has revealed a critical role of the $W/NPLY^{747}$ motif in β3 integrin signaling (LaFlamme et al., 1994; Ylänne et al., 1995; Schaffner-Reckinger et al., 1998), which further requires Rac1 GTPase activity (Berrier et al., 2000, 2002; Guillou et al., 2008). In addition, the kindlin adapter protein appears critical for integrin-dependent spreading, as kindlin-3 knockout prevents platelet spreading in vivo and in vitro and perturbs other integrin-dependent functions in the hematopoietic system (Moser et al., 2008, 2009). Kindlins enhance talin-mediated integrin activation while binding the membrane-distal $NITY^{759}$ motif and inter-NxxY region (Ma et al., 2008; Harburger et al., 2009). Mutation $S^{752}P$ in the latter binding motif causes loss of kindlin binding as well as Glanzmann's thrombasthenia (Chen et al., 1994; Ma et al., 2008; Moser et al., 2008; Harburger et al., 2009).

As a result of the close functional link between talin- and kindlin-mediated integrin activation and subsequent cell spreading and/or paxillin and FAK recruitment, the mechanism of integrin-mediated spreading has not yet been uncoupled from that of integrin activation. A major obstacle to resolving this issue is linked to the use of loss-of-function integrin mutations, which caused simultaneous failure of talin binding and loss of cell spreading. Thus, we decided to experimentally increase the talin–integrin affinity, to maintain robust cell–matrix adhesion (CMA), while screening for integrin mutations that failed to induce cell spreading. By creating β3 integrin chimeras with talin-binding peptides from layilin or PIPK1-γ, integrin–talin affinity increased by 20-fold, causing robust integrin activation but spreading only in the case of the layilin-based chimera. In this chimera, spreading, but not talin binding, was lost by a Tyr to Ala mutation in the conserved $W/NPLY^{747}$ motif. Loss of spreading correlated with the failure to recruit the signaling adapter protein paxillin to focal adhesions formed by these talin-bound chimeric integrins. Kindlin-binding integrin mutations also failed to induce cell spreading, despite the recruitment of integrins into focal adhesions. In addition, enhancing the integrin–talin affinity enabled focal adhesion formation on very soft fibronectin (FN) polyacrylamide gels but spreading only in the case of the layilin chimera. These data suggest that integrin activation and focal adhesion formation is controlled by the physical state of the ECM as well as talin and kindlin binding to integrins but that cell spreading and potentially other integrin-signaling events require the recruitment of signaling adapter proteins, such as paxillin to the integrin–talin–kindlin complex.

Results

Development of a β3-GFP-integrin–dependent cell-spreading assay

To quantify integrin signaling, we developed an integrin-dependent spreading assay (Fig. 1 A), by transiently expressing wild-type and mutant forms of a validated GFP-tagged mouse β3 integrin (Ballestrem et al., 2001). Specificity was obtained by transfecting a clone of NIH-3T3 fibroblasts that exhibits very low levels of endogenous β3 integrin, when compared with other mouse fibroblasts (Fig. 1 B and Fig. S1). However, these cells express endogenous α5β1 integrins, recognized by mAbs 9EG7 and HMβ1-1, binding only activated or all β1 integrins, respectively (Fig. 1 B). After transfection and FACS sorting for β3-GFP-integrin, cells were plated in serum-free medium on glass coverslips coated with 1 µg/ml vitronectin (VN), an αvβ3 integrin ligand that does not bind α5β1 integrins. The spreading kinetics was followed by phase-contrast microscopy (Fig. 1, C and D). To confirm nontoxicity of mutants, cells were plated on coverslips coated with 10 µg/ml FN, which induced spreading irrespectively of the transfected β3 integrin (Fig. 1 E). When compared with mock-transfected cells, which showed a delay in spreading of ∼60 min on VN, wild-type β3-GFP-integrin–transfected cells started to spread immediately, reaching half-maximal and complete spreading at 60 and 240 min, respectively (Fig. 1 D). This spreading was identical to anti-β3 sorted cells, transfected with nontagged mouse β3 integrin (Fig. S2), suggesting that the C-terminal GFP tag was not perturbing the integrin-spreading response (Ballestrem et al., 2001). In contrast to wild-type β3-GFP-integrin, the talin binding–deficient $Y^{747}A$ β3-GFP-integrin mutant prevented spreading for ≤2 h, resulting in 30% spreading at 6 h. However, after 15 h, cells were spread similarly to wild-type and mock-transfected cells, proposing that FN secretion and endogenous α5β1 integrins (Fig. 1 B) overcame the block in spreading on VN (Fig. 1, F and G).

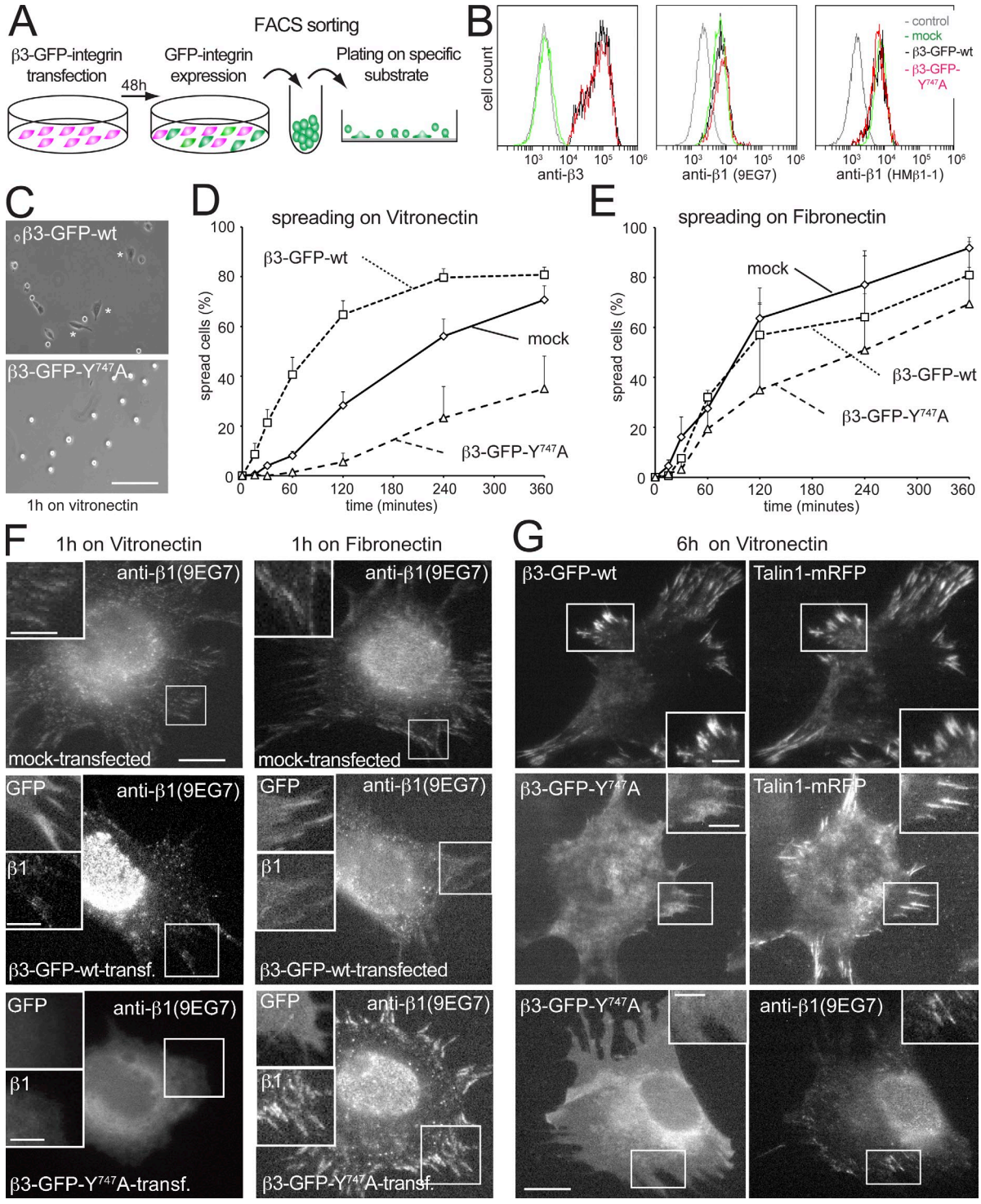

Figure 1. **Analysis of β3-GFP-integrin–dependent cell spreading.** (A) Illustration of the spreading assay. NIH-3T3 fibroblasts were transiently transfected with wild-type or mutant mouse β3-GFP-integrin constructs and FACS sorted before plating onto 1 μg/ml VN- or 10 μg/ml FN-coated glass coverslips. (B) FACS analysis for cell surface expression of β3 and β1 integrin (activated [9EG7] and total [HMβ1-1] population) in mock, wild-type, and $Y^{747}A$ mutant β3-GFP-integrin–transfected NIH-3T3 cells. Panels show representative results from a single experiment out of three repeats. (C) Phase-contrast images of NIH-3T3 cells expressing wild-type or $Y^{747}A$ mutant β3-GFP-integrin after plating for 1 h on VN. Bright and round cells were counted as nonattached, whereas dark-appearing cells (asterisks in C) were counted as spread to obtain curves as depicted in D and E. (D and E) Spreading curves of transfected NIH-3T3 cells on VN (D) and FN (E), expressing the indicated construct. (F) Epifluorescence images of mock or β3-GFP-integrin–transfected NIH-3T3 cells plated for 1 h on VN or FN and stained for substrate-bound β1 integrin revealed by mAb 9EG7 staining. Note the recruitment of β1 integrins into CMAs, in mock-transfected cells on both VN and FN substrates, and absence of CMA-recruited β1 integrins in wild-type or $Y^{747}A$ mutant β3-GFP-integrin–expressing cells on VN. On FN, wild-type, but not $Y^{747}A$, β3-GFP-integrin prevented the recruitment of β1 integrin into CMAs. (G) TIRF images of wild-type or $Y^{747}A$ β3-GFP-integrin cotransfected with talin1-mRFP or stained for endogenous ligand-bound β1 integrins after 6 h of spreading on VN. Insets correspond to magnified views of the boxed area as well as the respective GFP signal in this location, when indicated. wt, wild type. Bars: (C) 100 μm; (F and G, main images) 10 μm; (F and G, insets) 5 μm.

Spreading defect of $Y^{747}A$ mutant β3 integrins on VN but not FN

To analyze integrin recruitment to CMAs during the initial spreading phase, ligand-bound α5β1 integrin was detected with mAb 9EG7 staining, and clustered αvβ3-GFP-integrin was detected by epifluorescence and total internal reflection fluorescence (TIRF) imaging (Fig. 1, F and G). Although mAb 9EG7 staining was detected in CMA in the few mock-transfected cells spread on VN after 1 h, 9EG7 staining appeared diffuse in wild-type β3-GFP-integrin–transfected cells spread on VN and FN (Fig. 1 F). Thus, at early time points, high levels of β3-GFP-integrin prevented recruitment of endogenous α5β1 integrin into CMAs on both ligands. In contrast, the $Y^{747}A$ mutant β3-GFP-integrin failed to cluster, blocked the formation of α5β1-containing CMAs, and prevented initiation of spreading when plated for 1 h on VN (Fig. 1 F, bottom left image). However, the same cells recruited α5β1 into CMAs when spread on FN (Fig. 1 F). These data suggested ligand-specific initiation of spreading via αvβ3-GFP-integrin on VN, which was not compensated by endogenous integrins (such as α5β1) at early time points. After 6 h on VN, wild-type β3-GFP-integrin colocalized with talin1-mRFP (Fig. 1 G), whereas $Y^{747}A$ mutant β3-GFP-integrin remained diffuse in the membrane without colocalization to talin1-mRFP or mAb 9EG7-reactive (α5β1 containing) CMAs (Fig. 1 G). This suggests that cells secreted their own FN, which rescued spreading in cells expressing talin binding–defective integrins by endogenous α5β1 integrins.

Talin binding and integrin activation are critical for spreading initiation

To characterize additional β3 integrin tail residues required for cell spreading on VN, we expressed several talin-binding variants with mutations affecting both the W/NPLY^{747} and membrane-proximal motifs. Initiation of spreading was suppressed with all mutations known to affect talin binding to β3 integrin, including $Y^{747}A$, $L^{746}A$, $W^{739}A$, $W^{739}A/Y^{747}A$, $E^{726}K$, and $F^{730}A$ (Fig. S2). The $W^{739}A/Y^{747}A$ double mutant had the strongest negative effect on cell spreading, confirming the link between talin binding and cell spreading (Fig. S2). In contrast, the mutational unclasping of the inhibitory salt bridge ($D^{723}A$), which enhances integrin activation and clustering (Tadokoro et al., 2003; Cluzel et al., 2005), slightly enhanced the spreading response on VN (Fig. S2). This confirmed the link between talin-mediated integrin activation, clustering, and spreading.

High-affinity talin–integrin association does not guarantee initiation of cell spreading

Because integrin–talin interaction appeared to be critical for integrin-mediated spreading, we searched for ways to experimentally dissociate talin-mediated integrin activation from the mechanisms that induce integrin-mediated spreading (Fig. S2). To maintain integrin activation and talin linkage even in the absence of spreading, we decided to create integrin mutants with enhanced talin-binding affinity. We designed chimeric β3-GFP-integrins, in which the W/NPLY^{747} motif (K_d = 0.3 mM; Anthis et al., 2010) was replaced with known high-affinity talin-binding motifs. Based on the interactions of layilin and PIPKI-γ with the talin F3/phosphotyrosine-binding (PTB) domain (Barsukov et al., 2003; de Pereda et al., 2005; Kong et al., 2006; Wegener et al., 2008), two chimeras, β3-VE (layilin chimera; similar to a β1D-derived chimera with K_d = 17 nM for talin2; Anthis et al., 2010) and β3-SPLH (PIPKI-γ chimera; K_d = 0.27 µM for a nonphosphorylated peptide; de Pereda et al., 2005), were designed (Fig. 2, A and B). Although these chimeras led to integrin activation (Fig. 2 E) and colocalization with talin1-mRFP in CMAs (Fig. 2, F and G), only the β3-VE chimera induced spreading on VN comparable to β3 wild type (Fig. 2 C). In stark contrast, the β3-SPLH chimera, despite enhanced binding to talin, prevented spreading similar to the $Y^{747}A$ mutant (Fig. 2 C).

Y^{747} is required for spreading but not for high-affinity talin binding of the β3-VE chimera

To further characterize the spreading behavior and high-affinity talin interactions of the β3-VE chimera, we asked whether Y^{745} in the WVENPLY^{745} sequence plays a similar role in spreading initiation and talin binding as Y^{747} in the original β3 integrin sequence. To analyze this, we created the VE/$Y^{745}A$ mutant (WVENPLA^{745}K), which showed reduced activation levels in respect to VE, which were however comparable to wild-type β3-GFP-integrin (Fig. 3, A and B). Nevertheless, the $Y^{745}A$ mutation in the β3-VE chimera blocked spreading similar to the $Y^{747}A$ mutation in β3 (Fig. 3 C). In contrast to the $Y^{747}A$ mutant, GST–talin head pulled down the β3-GFP-VE/$Y^{745}A$ mutant comparable to β3-wt, β3-SPLH, and β3-VE (Fig. 3 D and Fig. S3), despite variations of integrin expression levels observed in this experiment. To provide a more quantitative measure of binding affinities of these mutants, we performed biosensor experiments with immobilized, His-tagged talin head (1–406 aa) and purified wild-type or mutant GST–β3-tail fusion proteins. These experiments revealed a ∼20-fold higher affinity of the β3-VE chimera and a ∼10-fold higher affinity of the β3-VE/$Y^{745}A$ mutant over wild-type β3-tail. (Fig. 3 E), demonstrating that Y^{745} is no longer critical for talin binding in the context of the β3-VE chimera. Consistent with strong talin binding, the β3-VE/$Y^{745}A$ mutant colocalized with talin1-mRFP (Fig. 3 F). This links talin binding to integrin activation and recruitment to focal adhesions but fails to reveal a direct role of talin during integrin signaling and spreading on VN.

Mutations of kindlin-binding motifs affect cell spreading

Kindlin-3 is required for platelet spreading (Moser et al., 2008). Although kindlins do not interact with the NPLY^{747} talin-binding motif, kindlins stimulate talin-mediated integrin activation (Ma et al., 2008), which could be essential to subsequent initiation of cell spreading. To study the role of kindlin in the regulation of cell spreading, both the distal NITY^{759} ($Y^{759}A$) and inter-NxxY ($S^{752}P$) kindlin-binding motifs (Ma et al., 2008; Moser et al., 2008) were mutated. Expression of both the β3-$Y^{759}A$- and β3-$S^{752}P$-GFP-integrin was slightly lower than wild type (Fig. 4 A) but caused strong β3 integrin activation defects

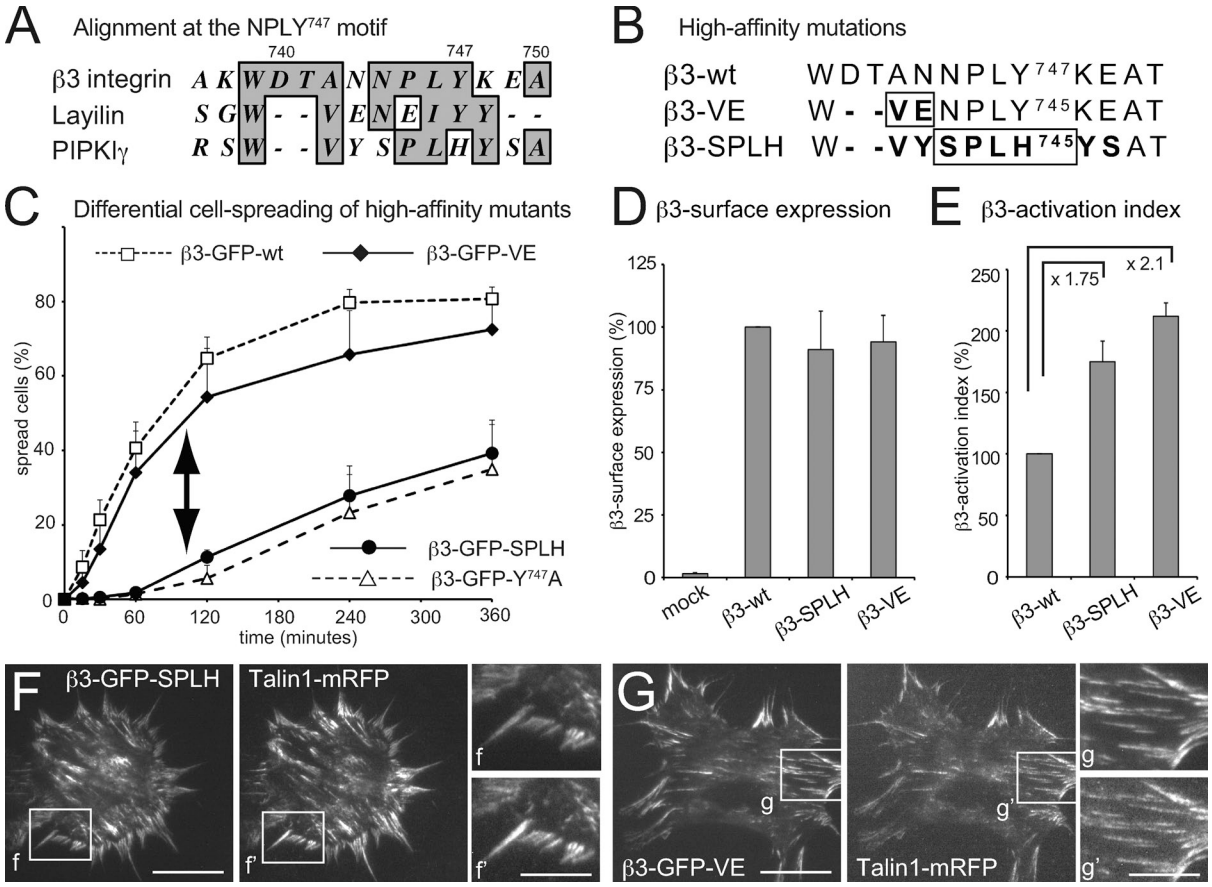

Figure 2. **Differential cell spreading by high-affinity talin-binding β3-GFP-integrins.** (A) Sequence alignment of β3 integrin and the high-affinity talin-binding sequences from layilin and PIPKI-γ. Gray shading defines identical or conserved residues. (B) Sequences of the chimeric β3-GFP-integrins (β3-VE with the VE motif from layilin and β3-SPLH derived from PIPKI-γ). Bold indicates mutated residues, and boxed letters correspond to the name of the integrin chimeras. (C) Spreading curves of NIH-3T3 cells transiently transfected with β3-GFP-VE and β3-GFP-SPLH chimera on VN and comparison with wild-type and spreading-deficient $Y^{747}A$ mutant β3-GFP-integrin. Double arrow indicates differential spreading of high-affinity chimeras. (D and E) β3 integrin cell surface expression levels of β3-GFP-chimera in NIH-3T3 cells (D) and increases in the β3 integrin activation index in the chimeras (E). Numbers indicate fold increase in the activation index. (F and G) Representative TIRF images of NIH-3T3 cells spread for 6 h on 1 µg/ml VN, transiently transfected with β3-GFP-SPLH (F), β3-GFP-VE chimera (G), and talin1-mRFP. Note the talin1 colocalization with both chimeras, despite a delay in cell spreading for β3-GFP-SPLH. Error bars show standard error. wt, wild type. Bars: (main images) 25 µm; (insets) 12.5 µm.

(Fig. 4 B). Although β3-S^{752}P-GFP-integrin–expressing cells failed to cluster and to spread on VN, β3-Y^{759}A-GFP-integrin–transfected cells spread similarly to mock-transfected cells (Fig. 4 C) and displayed some integrin recruitment into CMAs at 6 h (Fig. 4, D and F). However, when combined with the integrin-activating D^{723}A mutation, which enhanced integrin clustering (Cluzel et al., 2005) and ligand binding in a talin-dependent manner (Tadokoro et al., 2003), both double mutants were highly activated and co-clustered with talin1-mRFP (Fig. 4, B, E, and G). This finding proposes that integrin activation and clustering is mainly regulated by talin-mediated unclasping of integrins at their juxtamembrane region. Importantly, although the D^{723}A/Y^{759}A mutant induced normal spreading, the D^{723}A/S^{752}P mutant failed to support cell spreading, despite localization to CMAs, reminiscent of the VE/Y^{745}A mutant chimera (Fig. 4 C). This proposes that the C-terminal integrin tail is important for talin activation (NITY^{759} motif) as well as for cell spreading (inter-NxxY region). Whether this is caused by kindlin binding or linked to an alternative integrin-binding adapter needs to be shown.

Spreading-defective, high-affinity talin-binding integrins fail to recruit paxillin

Because integrin mechanosensing is associated with FAK phosphorylation (Friedland et al., 2009), which colocalizes with phosphopaxillin in nascent adhesions (Choi et al., 2011), we asked how paxillin, which is a master regulator of adhesion-mediated signaling and actin remodeling (Deakin and Turner, 2008, 2011), is recruited to spreading-defective integrins. Thus, endogenous paxillin localization was studied by TIRF immunofluorescence in β3-GFP-integrin–transfected cells spreading on VN (Fig. 5). Paxillin efficiently localized to CMAs formed by wild-type and β3-VE chimera at 1 and 4 h (Fig. 5, A, B, and E). In contrast, paxillin colocalized only partially with β3-GFP-SPLH chimera and β3-GFP-VE/Y^{745}A mutant integrins in lamellipodial protrusions of spreading cells (Fig. 5, C–E). Determination of the Mander's colocalization coefficient revealed consistently fewer β3-GFP-integrin clusters at sites of paxillin staining (Fig. 5 E), suggesting that paxillin fails to be recruited to spreading-incompetent, but talin-bound, integrins. Accordingly, such reduced recruitment could prevent or slow down the reinforcement of

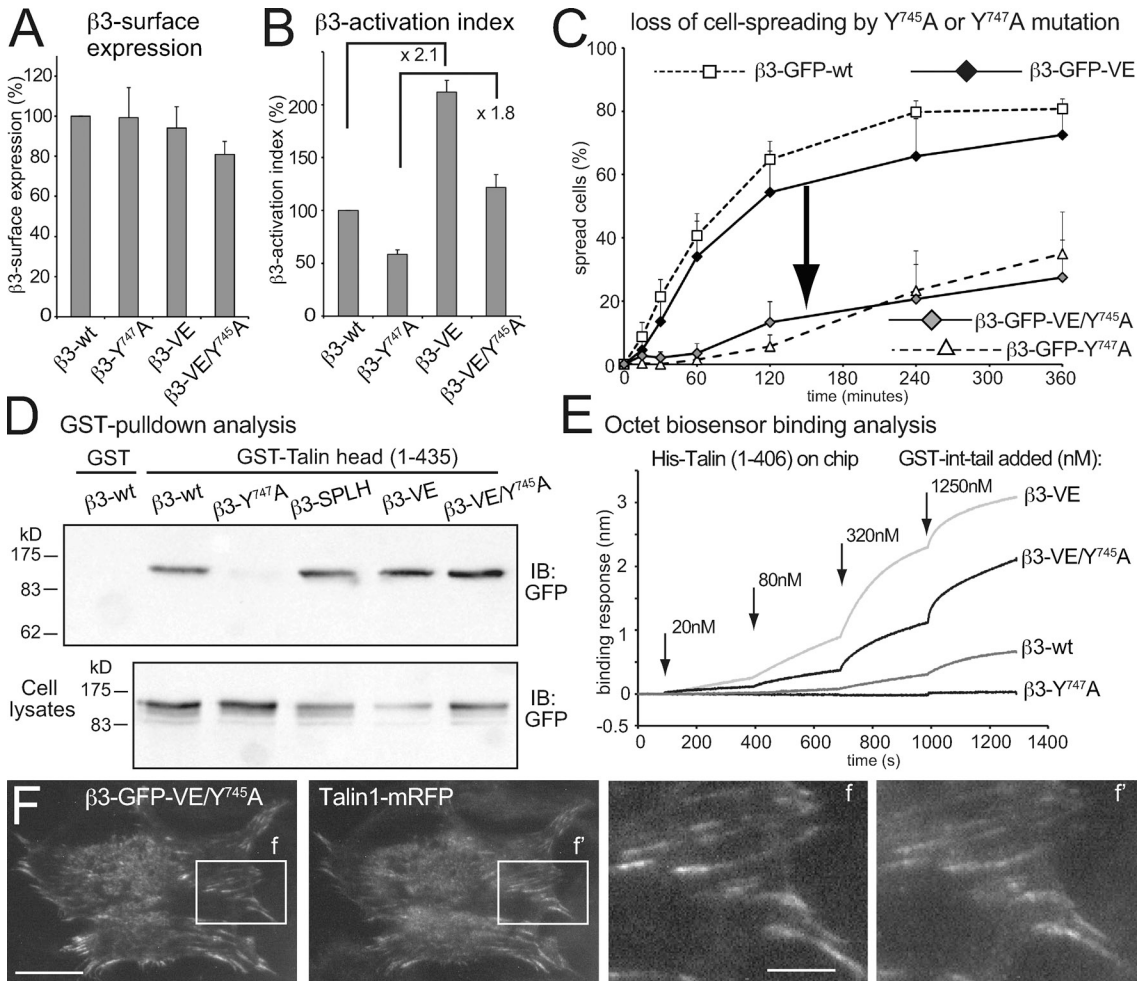

Figure 3. **Loss of cell spreading in the β3-GFP-VE/Y^{745}A chimera despite high affinity talin binding.** (A) Cell surface expression levels of β3-GFP-VE chimera and β3-GFP-VE/Y^{745}A double mutant. (B) β3 integrin activation index in the presence of Y^{745}A and Y^{747}A mutations in transiently transfected NIH-3T3 cells. (C) Spreading curves of NIH-3T3 cells transiently transfected with the constructs used in A and B. Note the reduced cell spreading with the double mutant (β3-GFP-VE/Y^{745}A). Arrow indicates the loss of cell spreading induced by the Y^{745}A mutation. (D) Pull-down assay using GST–talin head fusion protein is shown, and lysates from COS-7 cells, which were transiently transfected with wild-type, Y^{747}A, SPLH, VE, and VE/Y^{745}A mutant β3-GFP-integrins. Note the equal pull-downs of the β3-VE integrin despite lower concentrations in lysates. The full blots are shown in Fig. S3. (E) Octet biosensor analysis of the interaction between GST-β3-tail chimeras and Ni-NTA sensor functionalized with His-tagged talin head (1–406 aa). (F) Representative TIRF images of NIH-3T3 cells spread for 6 h on 1 µg/ml VN, transiently transfected with β3-VE/Y^{745}A-GFP-integrin chimera and talin1-mRFP. Error bars show standard error. IB, immunoblot; wt, wild type. Bars: (F) 25 µm; (f and f′) 10 µm.

nascent adhesions, leading to the observed delay in cell spreading (Fig. 5 F).

Although the absence of paxillin is a valid explanation for the delay in spreading, the analysis is flawed by endogenous FN secretion and α5β1 integrin recruitment to lamellipodia, which could support substrate binding and integrin signaling during spreading. Thus, to circumnavigate this obstacle, and to physically separate α5β1 from αvβ3 integrin–mediated signaling during spreading, cells were plated on patterned substrates consisting of FN patches surrounded by a VN-coated surface (Fig. 6 E). Irrespective of the expressed β3-GFP-integrin construct, cells spread on this pattern, using endogenous α5β1 integrins for adhesion formation (paxillin recruitment) on FN patches. In the presence of wild-type β3-GFP-integrin, cells preferably spread on VN-coated surfaces, efficiently recruiting paxillin to CMAs (Fig. 6 A). When CMAs extended over both VN- and FN-coated surfaces, paxillin was recruited irrespective of the substrate borders, whereas β3-GFP-integrin remained restricted to VN surfaces (Fig. 6 A, inset). A similar situation was seen with the β3-GFP-VE chimera, with the difference that more GFP staining (integrin fusion partner) was detected on FN-coated surfaces (Fig. 6 B). However, a different image was seen in cells transfected with the β3-GFP-SPLH chimera (Fig. 6 C) or β3-GFP-VE/Y^{745}A mutant (Fig. 6 D). GFP-positive CMAs localized on VN surfaces failed to recruit paxillin, whereas paxillin-enriched CMAs located on FN patches were devoid of GFP fluorescence (Fig. 6, C and D). This shows that β3-SPLH chimera and the β3-VE/Y^{745}A mutant interact with VN, talin, and F-actin but fail to recruit paxillin, potentially causing the observed defect in cell spreading on VN.

Separation of integrin-dependent adhesion and mechanosensing on soft substrates

In addition to spreading, integrin signaling operates during mechanosensing, during which a tension-controlled α5β1 integrin

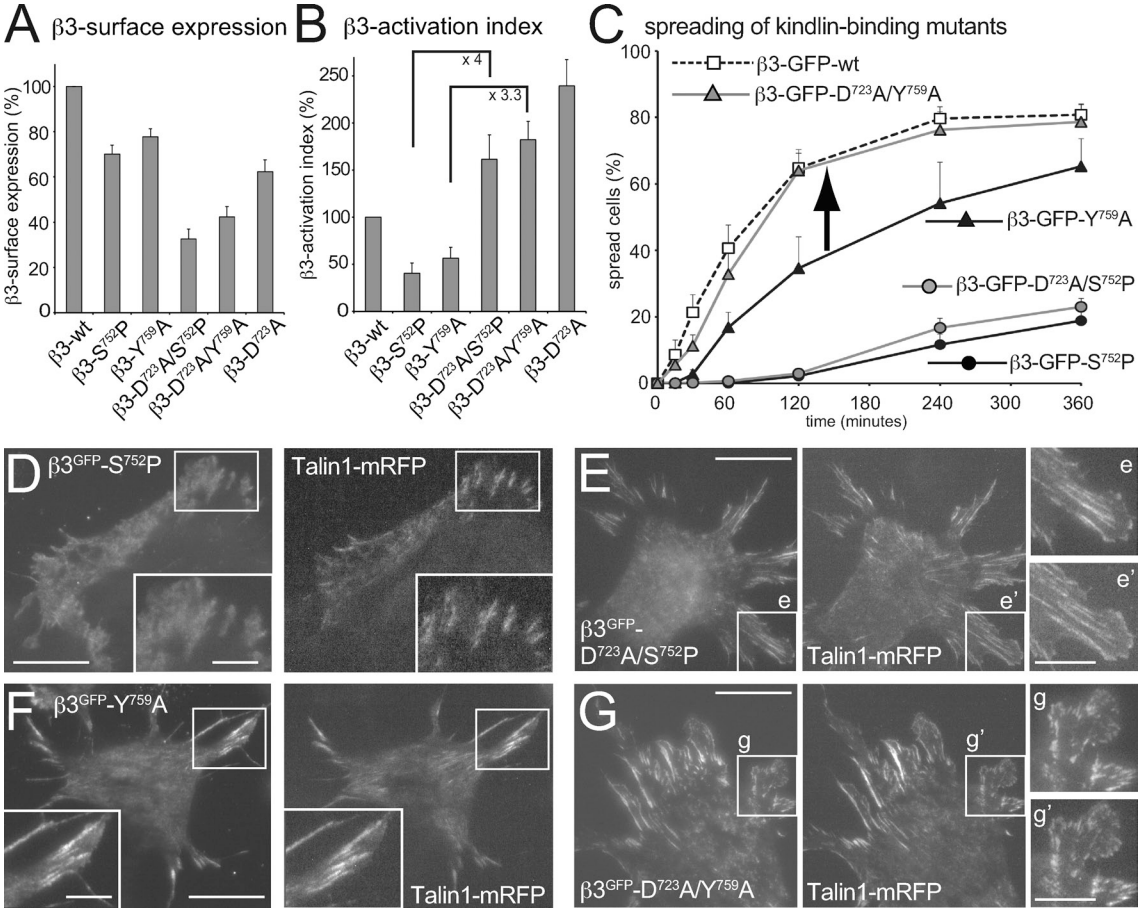

Figure 4. **Cell spreading analysis of kindlin binding–deficient β3 integrin mutants.** (A) Cell surface expression levels of individual β3-S^{752}P- and β3-Y^{759}A-integrin mutants and their respective levels when combined with the activating D^{723}A mutation. (B) β3 integrin activation index of the mutations shown in A. Numbers indicate fold increase in activation index caused by the D^{723}A mutant. (C) Spreading curve of NIH-3T3 cells transfected with kindlin binding–deficient (S^{752}P and Y^{759}A) β3-GFP-integrin alone or in combination with the activating D^{723}A mutation (D^{723}A/S^{752}P and D^{723}A/Y^{759}A). The arrow indicates the increase in cell spreading by the D^{723}A mutation. (D–G) Representative TIRF images of NIH-3T3 cells spread for 6 h on 1 µg/ml VN, transiently transfected with β3-S^{752}P (D), β3-Y^{759}A (F), and respective double mutant β3-D^{723}A/S^{752}P- or β3-D^{723}A/Y^{759}A-GFP-integrin together with talin1-mRFP. Note that despite lack of spreading, efficient colocalization with talin1-mRFP can be detected for the β3-GFP-D^{723}A/S^{752}P-integrin mutant (E). Insets are magnifications of the boxed regions. Error bars show standard error. wt, wild type. Bars: (main images) 25 µm; (insets) 10 µm.

switch regulates FAK signaling (Friedland et al., 2009). However, on soft FN-coated surfaces, this tensional switch fails, preventing full cell spreading and causing an absence of stress fiber formation below a substrate stiffness of 3 kPa (Yeung et al., 2005). Accordingly, reducing substrate stiffness will inactivate the signaling of endogenous α5β1 integrin, normally activated on rigid FN-coated substrates. To test whether a tension-mediated switch would also be relevant for αvβ3 integrins, we compared β3 integrin recruitment on glass coverslips covalently coated with FN, with that of 30 kPa polyacrylamide (PAA) gels. When compared with FN-functionalized glass, on which wild-type β3-GFP-integrin–transfected cells were well spread and recruited some β3-GFP-integrins into CMAs after 2.5 h of spreading (Fig. S4), β3-GFP-integrin enrichment in CMAs was rarely observed, and many cells showed reduced spreading and no discernable CMAs when plated on FN-coated PAA (30 kPa) gels. On the other hand, the activated β3-GFP-SPLH-integrin was enriched in focal adhesions on both FN-coated glass and PAA gels (Fig. S4). Similarly, the β3-GFP-VE chimera was strongly enriched in CMAs on FN-coated glass and easily detected on PAA gel surfaces (Fig. S4), suggesting that both the affinity between talin and integrins as well as the physical state of the extracellular ligand controls the conformation of the integrin and thereby its recruitment into CMAs.

To test whether high-affinity talin-binding integrins induce spreading on very soft substrates that would not allow β1-dependent spreading (<3 kPa; Yeung et al., 2005), spreading of β3-VE– and β3-GFP-SPLH–transfected fibroblasts was performed on soft (1.5 kPa) FN-coated PAA gels (Fig. 7). When plated for 2.5 h, efficient cell spreading, integrin clustering, and stress fiber formation was observed on both soft (1.5 kPa) and stiff (30 kPa) PAA substrates in the case of the β3-GFP-VE chimera (Fig. 7, A and C). However, cells transfected with the β3-GFP-SPLH chimera failed to completely spread and flatten on soft substrates, despite the recruitment of this integrin into CMAs (Fig. 7 B and Fig. S4). In addition, SPLH-transfected cells exhibited characteristic filopodial adhesions, containing clustered integrins linked to F-actin bundles (Fig. 7 B) but failed to spread and form actin stress fibers. In contrast, on stiffer (30 kPa)

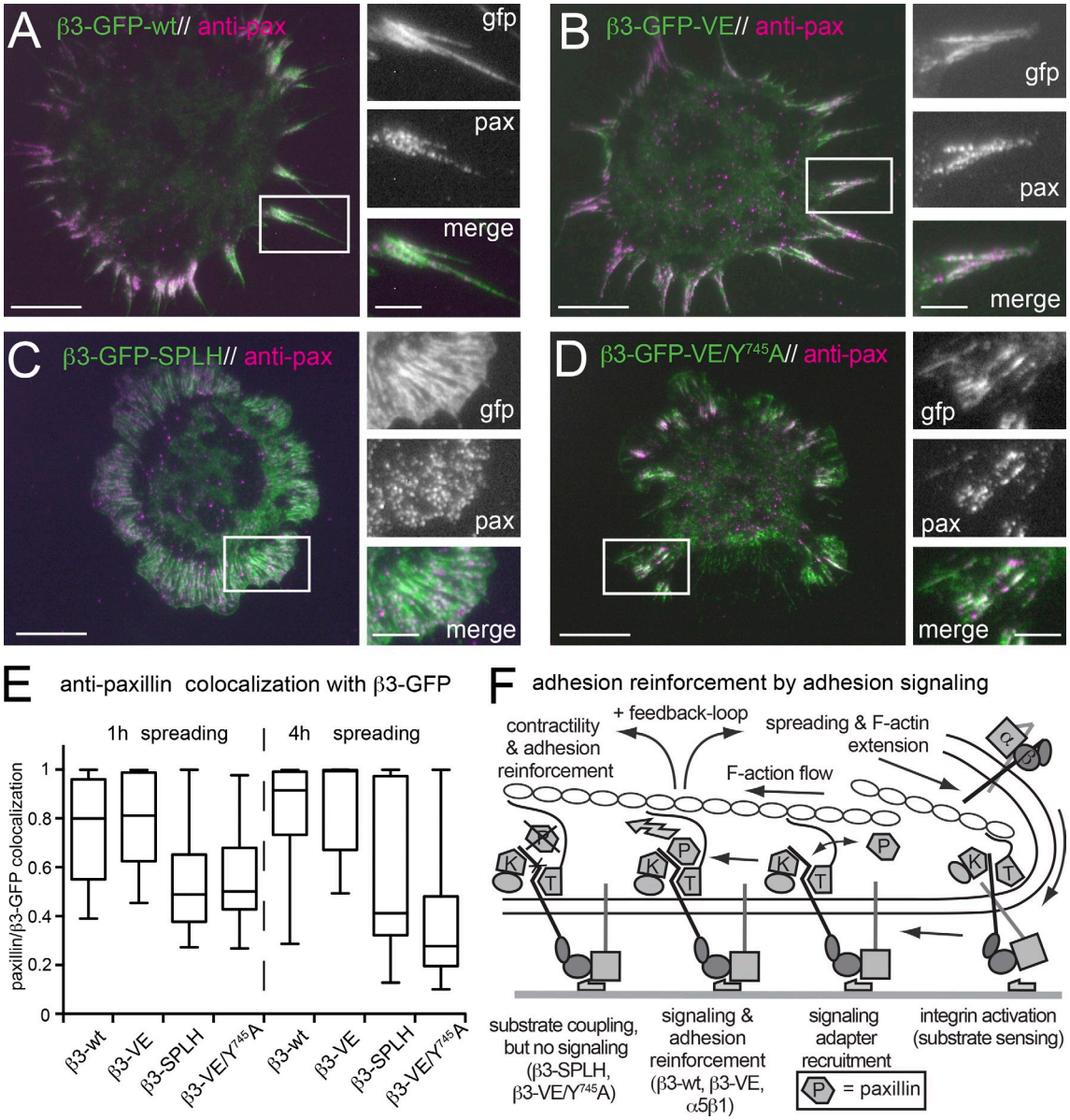

Figure 5. **Analysis of paxillin recruitment to wild-type and mutant β3-GFP-integrins.** (A–D) Merged TIRF images of NIH-3T3 cells spread for 1 h on 1 µg/ml VN-coated glass coverslips transiently transfected with wild-type β3-GFP-integrin (A), β3-GFP-VE (B), β3-GFP-SPLH (C), and β3-GFP-VE/Y^{745}A (D) chimera and stained for endogenous paxillin. Magnified views of the boxed areas in A–D showing the GFP (gfp) and antipaxillin (pax) signals. (E) Mean, box (±25%), and whisker (minimum/maximum) plot (n = 30–50 cells) of Mander's colocalization coefficients using automatic threshold of antipaxillin reactivity localized in GFP clusters. Note the colocalization of antipaxillin staining with β3-GFP-integrins in A and B but only partial overlap in C and D. (F) Schematic view of integrin activation, association with adapter proteins and positive feedback to reinforce CMAs during lamellipodial extensions, and absence of such reinforcement in integrins failing to recruit paxillin (T, talin; P, paxillin; K, kindlin). Images in A–D were taken from one out of three similar experiments. wt, wild type. Bars: (main images) 15 µm; (insets) 5 µm.

FN-coated PAA gels, on which endogenous α5β1 integrin signaling is active, cell spreading occurred and the β3-GFP-SPLH chimera localized to peripheral and central CMAs (Fig. 7 D and Fig. S4), associated with the formation of stress fibers. This demonstrates that the talin–integrin affinity controls the mechanical stability and tension range in which a given integrin–ligand combination is operational. On the other hand, integrin mechanosignaling requires recruitment of adapter proteins, such as paxillin, to appropriately presented $NPLY^{747}$ motifs, to induce spreading, mechanosensing, and the subsequent remodeling of the actin cytoskeleton.

Discussion

The causal link between the mechanical, integrin-mediated connection from the cytoskeleton to the ECM and reciprocal intracellular signaling is critical for morphogenesis and tissue homeostasis and is mirrored in concepts such as anoikis, metastasis (Zouq et al., 2009; Taddei et al., 2012), or FAK activation in cells exposed to rigid ECM (Paszek et al., 2005; Friedland et al., 2009). Here, we provide a model of how integrin-mediated adhesions recruit signaling adapter proteins such as paxillin to regulate cell spreading. We identified integrin mutants that, despite

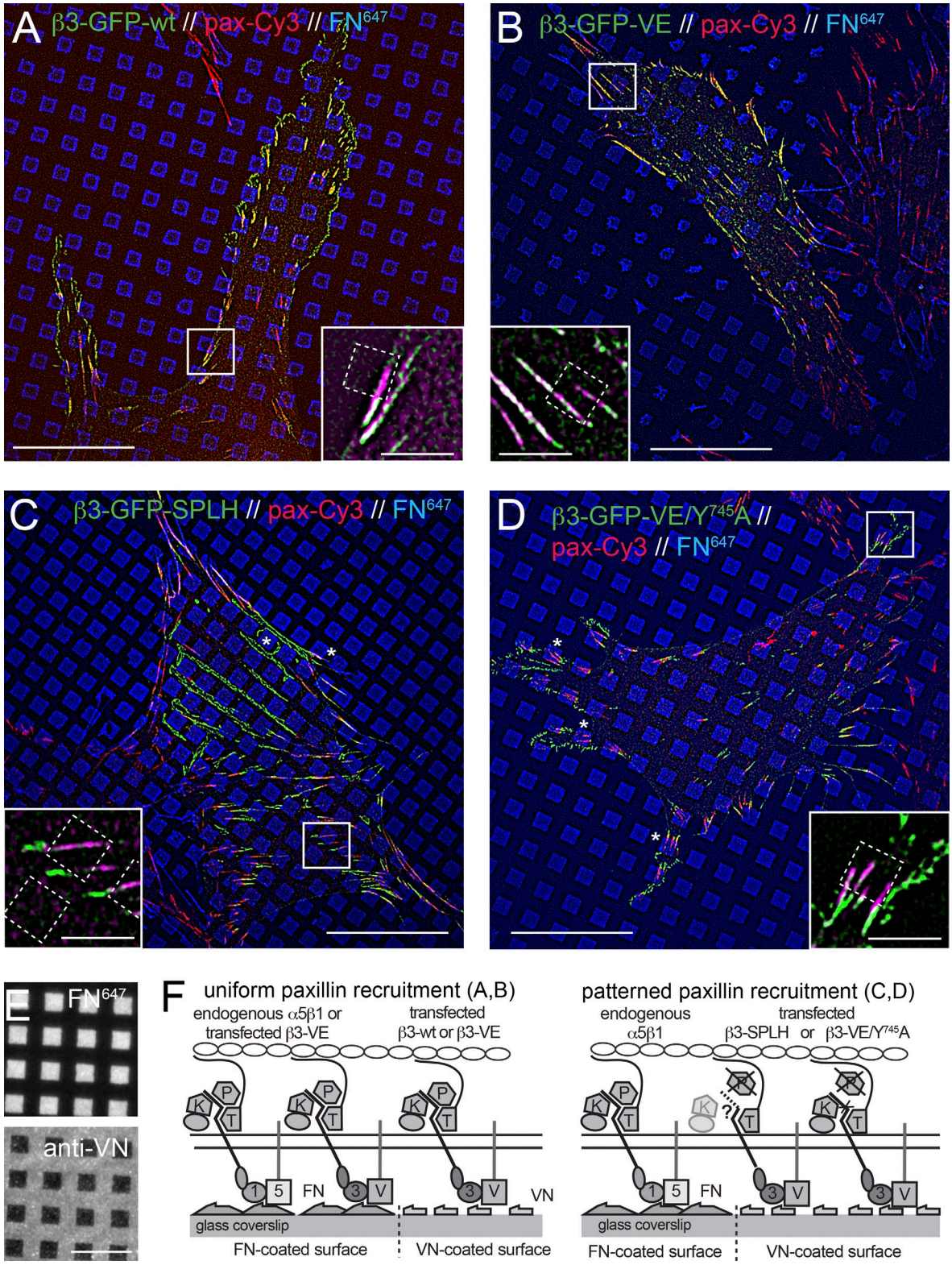

Figure 6. **Analysis of paxillin recruitment on FN/VN patterned substrates.** (A–D) Merged RGD planes of SIM images of NIH-3T3 cells spread for 4 h on FN/VN patterned substrates, representing the FN-coated surface (squares) and VN-coated surfaces without stain (grid). Cells express wild-type β3-GFP-integrin (A), β3-GFP-VE (B), β3-GFP-SPLH (C), and β3-GFP-VE/Y^{745}A (D), and antipaxillin reactivity. Magnified views of the boxed areas in A–D showing β3-GFP (in green) and antipaxillin staining (magenta) localized over FN-coated areas (dotted squares). Note the colocalization of antipaxillin staining with β3-GFP-integrins on VN and endogenous integrins on FN surfaces in A and B but the absence of antipaxillin staining in β3-GFP-integrin clusters on VN in C and D (asterisks). pax, paxillin. (E) Alexa Fluor 647–labeled FN- and anti-VN–stained patterns reveal the specificity of the coating strategy. (F) Schematic view of integrin signaling complexes in respect to integrin ligand and mutation. Integrins 1 and 5 correspond toα5β1, and 3 and V correspond to αvβ3. T, talin; P, paxillin; K, kindlin. Images in A–D were taken from one out of three similar experiments. Bars: (A–D) 20 µm; (E) 10 µm; (insets) 4 µm.

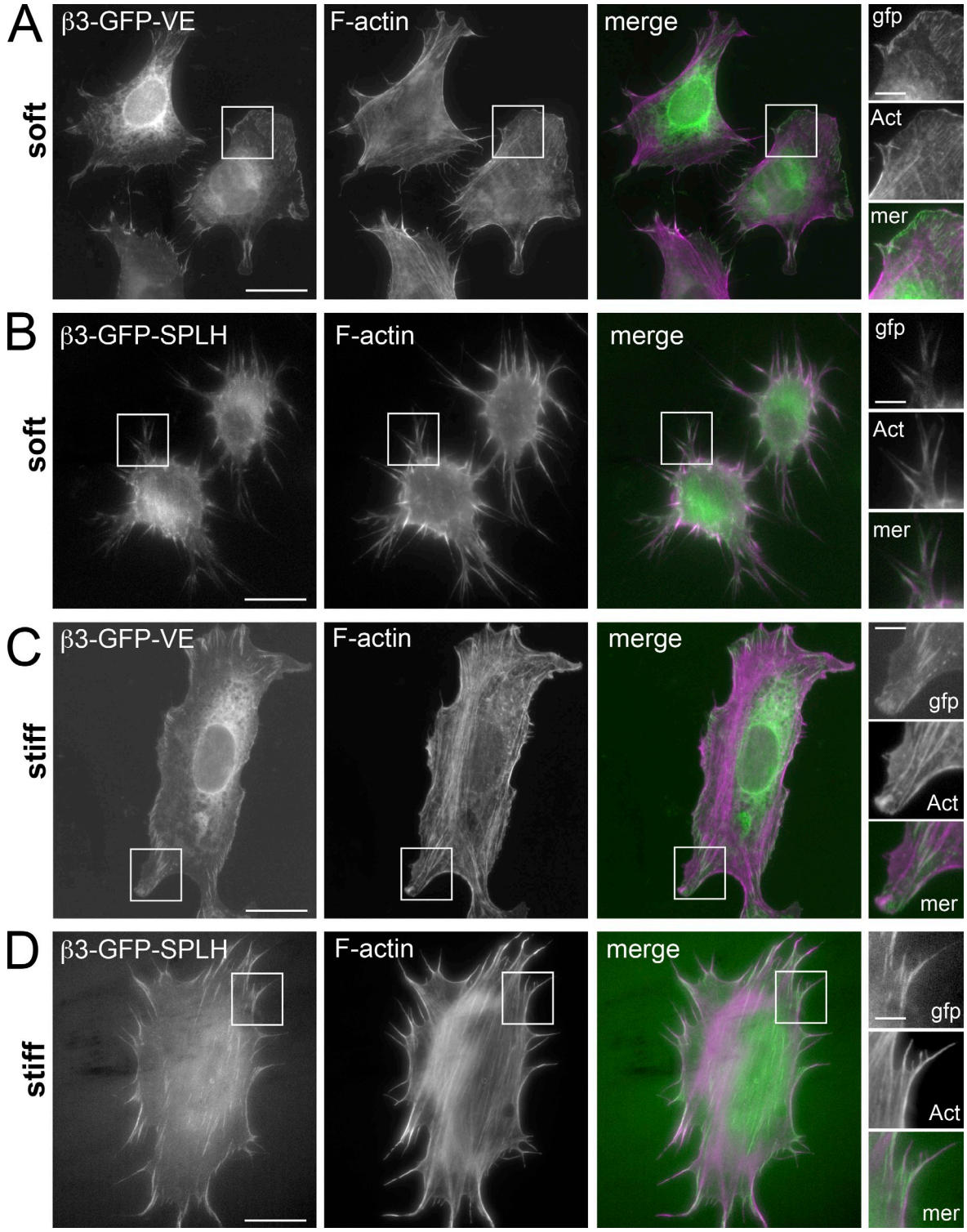

Figure 7. **Cell spreading on soft and stiff FN-coated PAA gels.** (A–D) ApoTome images of NIH-3T3 cells plated for 2.5 h on FN-functionalized (1 mg/ml) soft (1.5 kPa; A and B) and stiff (30 kPa; C and D) PAA gels, transiently transfected with β3-GFP-VE (A and C) and β3-GFP-SPLH chimeras (B and D). Cells were fixed and stained for F-actin (middle column) or imaged for GFP expression (left column). A magnified view of the boxed areas in A–D is shown on the right. Note the spreading of β3-GFP-VE–transfected cells on soft, FN-coated gels, whereas β3-GFP-SPLH accumulates in filopodial CMAs in round, nonspread cells. Please note that the UV-induced FN-coating method was used in this figure, which was repeated three times with similar phenotypes. Act, actin; mer, merge. Bars: (main images) 20 µm; (insets) 5 µm.

enhanced talin-binding and focal adhesion formation, failed to induce cell spreading and to recruit paxillin, a critical player in cell spreading, FAK activation, and regulation of Rho family GTPases (Wade et al., 2002; Deakin and Turner, 2008, 2011; Choi et al., 2011). We found that paxillin recruitment can be blocked by tyrosine mutation in the highly conserved talin-binding W/NPLY motif, even when bound to talin as in the VE/Y^{745}A chimera, suggesting that paxillin is recruited to β integrin tails when presented in a talin-bound state. In addition, adjacent β integrin tail sequences, known to bind kindlin are also required for cell spreading, thus proposing an explanation for the critical role of kindlins in immune defense, morphogenesis, and tumor growth (Moser et al., 2009; Pluskota et al., 2011; Sin et al., 2011). Furthermore, high-affinity talin-binding integrins induced cell adhesion and spreading, on soft, spreading-repellent ECM, proposing that mechanosensing of the ECM is directly linked to the stability of the integrin–talin complex and its ability to recruit signaling adapter proteins. These findings are key for evaluating and predicting the behavior of normal and tumor cells in response to pathological changes in matrix stiffness (Paszek et al., 2005; Engler et al., 2006), while offering new therapeutic strategies to differentially controlling integrin-mediated adhesion versus adhesion signaling.

Linking the integrin–talin–kindlin complex to cell spreading

Talin has emerged as the critical regulator of integrin activation and clustering (Tadokoro et al., 2003; Saltel et al., 2009). In addition, knockdown of talin or cell type–specific knockouts demonstrated a critical role in adhesion signaling, synergies with growth factors, and cell spreading (Miyamoto et al., 1995, 1996; Monkley et al., 2000, 2011; Petrich et al., 2007b). Moreover, the correlation between talin- and kindlin-mediated αIIbβ3 integrin activation, platelet spreading, and blood clotting proposes that the integrin–talin–kindlin complex induces intracellular signaling (Montanez et al., 2008; Moser et al., 2008, 2009). Interestingly, distinct platelet-spreading and bleeding phenotypes are observed between two β3 integrin mutants similarly defective in talin binding (Y^{747}A, strong bleeding defect, and L^{746}A, weak effect; Petrich et al., 2007a). In light of our data, these phenotypes might be caused by defects in integrin-mediated spreading.

Kindlins contribute to integrin activation (Ma et al., 2008), which involves binding to the inter NxxY region and distal NxxY motif (Bledzka et al., 2012; Yates et al., 2012). However, kindlins also mediate integrin signaling because the deletion of kindlin-2 in embryonic stem cells blocks spreading even in the presence of Mn^{2+}-activated integrins (Montanez et al., 2008). Thus, we propose that the distinct roles of kindlin in integrin activation and signaling are reflected by the Y^{759}A and S^{752}P mutations, respectively, showing differing phenotypes when combined with the activating D^{723}A mutation (Fig. 4 C). However, whether loss of kindlin interaction is indeed responsible for the phenotypes of these mutants needs to be determined.

Recruitment of signaling adapters and mechanosensing

Although a paxillin domain deletion study identified LIM (Lin-11, Isl-1, and Mec-3) domains 2 and 3 as the focal adhesion–targeting site, it is still not understood how paxillin is recruited to focal adhesions (Brown et al., 1996; Deakin and Turner, 2008). In fact, the absence of paxillin recruitment to lamellipodia in talin knockdown cells suggested that talin could be involved in paxillin recruitment (Zhang et al., 2008). Our data suggest that paxillin is recruited in a kindlin-regulated manner, either directly or indirectly to an interface formed by the talin-bound NPLY peptide. Although paxillin is recruited through its C-terminal LIM domains, the N-terminal LD domains can interact with multiple structural and signaling focal adhesion proteins, such as vinculin, parvin, FAK, and the GIT–PIX–PAK–NCK complex, creating an integrin-bound signaling nexus (Deakin and Turner, 2008). Moreover, phosphorylation of paxillin is required for FAK recruitment to nascent adhesions (Choi et al., 2011), suggesting that paxillin targets FAK to focal adhesions.

In contrast to this model, it was recently proposed that FAK recruits talin to nascent adhesions (Lawson et al., 2012). However, this is not consistent with FAK recruitment to integrin–talin complexes in filopodia (Partridge and Marcantonio, 2006) and the localization of FAK and vinculin to CMAs in response to the C-terminal talin rod domain (Wang et al., 2011). The talin rod domain exhibits numerous vinculin binding sites (Gingras et al., 2005), which are activated by mechanical force (Hytönen and Vogel, 2008; del Rio et al., 2009), thereby linking mechanosensing and FAK phosphorylation at Y^{397} to tensional stress along the ECM–integrin–talin–F-actin axis (Shi and Boettiger, 2003). Notably, our data also explain the phenotype of the *myospheroid*^{XRO4} mutant in *Drosophila melanogaster*, lacking both NPXY motifs but retaining the membrane-proximal talin–integrin binding site, which enables recruitment of talin but not that of paxillin to muscle attachment sites (Tanentzapf and Brown, 2006).

In addition to the cytoplasmic tail of integrins, the synergy site in FN, as well as the catch bond of the α5β1 integrin, is involved in mechanosensing, during which α5β1 integrin is a specific force transducer that can induce FAK signaling (Friedland et al., 2009; Kong et al., 2009; Boettiger, 2012). Modifying the cell type–specific force regimen by either softening or stiffening the ECM affects spreading and adhesion signaling (Yeung et al., 2005) as well as the differentiation of stem cells (Engler et al., 2006). Different adhesion strength between α5β1 and αvβ3 led to the proposal that α5β1 is mainly adhesive, whereas αvβ3 mediates mechanosensing (Roca-Cusachs et al., 2009). However, this idea contrasts with a study showing mechanosensing activities for both integrins (Shi and Boettiger, 2003). Thus, it is possible that these two integrins work under different force regimes. Although αvβ3 integrin enables spreading on stiff substrates, such as bone matrices and cross-linked tumor stroma (Paszek et al., 2005), α5β1 integrin functions within soft ECM conditions. That the β3-VE-integrin induces robust cell spreading on soft FN proposes that high talin–integrin affinity can compensate for weakly tethered integrin ligands, thus tuning mechanosensing to a different tensional state of the ECM.

Mechanism of talin-mediated, integrin-dependent cell spreading

As a result of several nuclear magnetic resonance (NMR) and crystal structures of the talin F3 (PTB) domain bound to

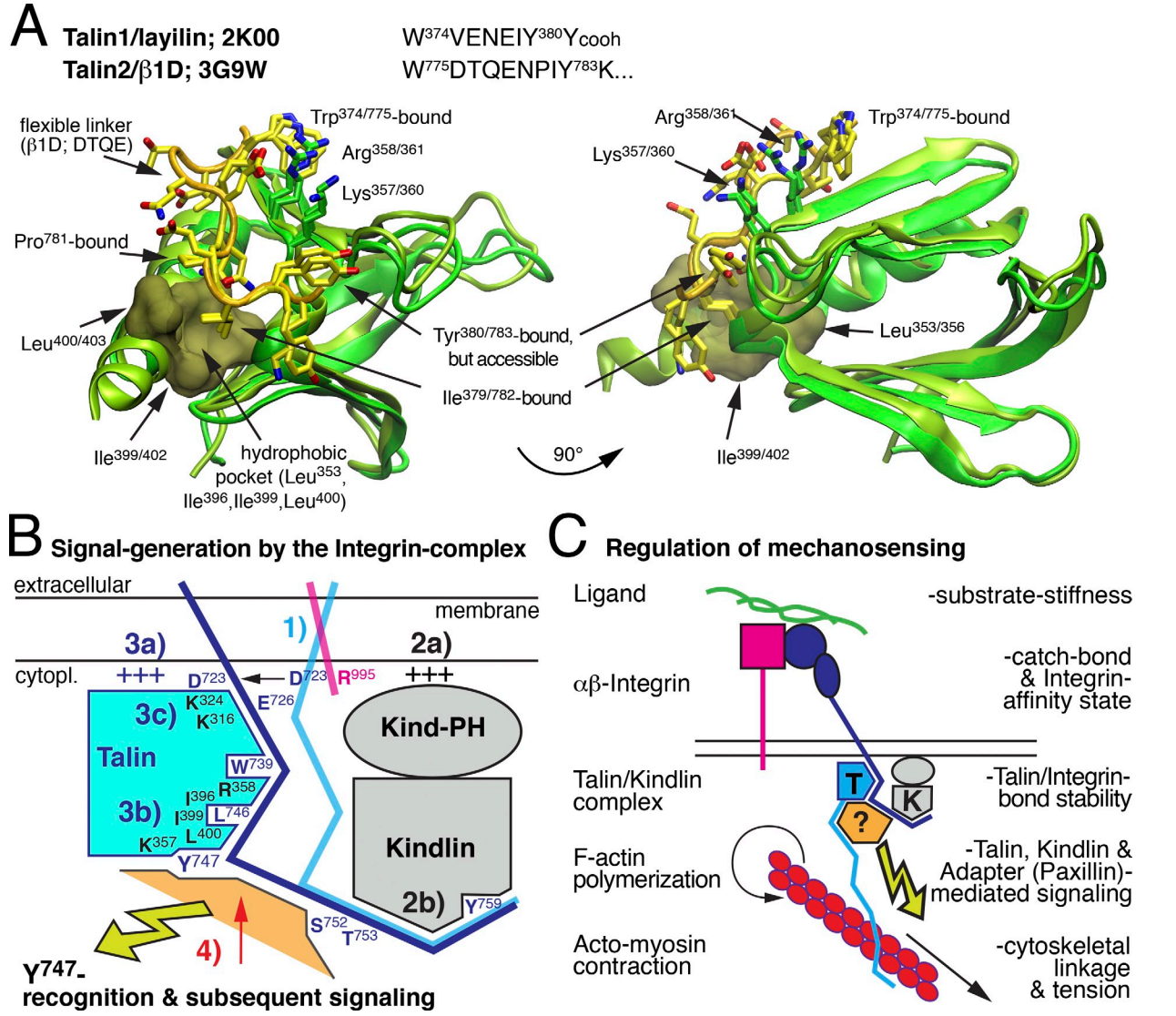

Figure 8. **Model of the integrin–talin–kindlin signaling complex.** NMR and crystal structures of the talin F3 (PTB) domain bound to different talin-binding peptides. (A) NMR structure of the talin1/layilin (Protein Data Bank accession number 2K00; Barsukov et al., 2003) and that of the talin2–β1D complex (Protein Data Bank accession number 3G9W; Anthis et al., 2009). In both structures, the conserved $Trp^{374/775}$ is bound next to $Arg^{358/361}$ of talin1/2, whereas the Ile residue of the tripeptides N-E-I and N-P-I is bound to a hydrophobic pocket formed by residues $Leu^{353/356}$, $Ile^{396/399}$, $Ile^{399/402}$, and $Leu^{400/403}$ of talin1/2, respectively. Between these motifs, a tightly bound dipeptide (V-E; layilin) or flexible linker (D-T-Q-E; β1D) makes electrostatic contacts with $Arg^{358/361}$ and $Lys^{357/360}$ residues. This particular binding mode places $Tyr^{380/783}$ into a shallow pocket, creating a surface-exposed hydrophobic surface. (B) Model of the signaling mechanisms induced by integrin binding to talin and kindlin, exposing Y^{747} for binding to a signaling adapter protein. Numbers 1–4 indicate different conformational states of the β3 integrin peptide (1) bound to the αv integrin tail, (2) recruitment of kindlin to the membrane (2a) and binding to the distal $NITY^{759}$ motif (2b), (3) interaction of talin with $PI(4,5)P_2$ lipids (3a), the $W/NPLY^{747}$-motif (3b), and binding at the membrane-proximal (D^{723} and E^{726}) motif to unclasp the integrins (3c), and (4) talin surface exposure of Y^{747} for recruitment of a signaling adapter. (C) Model of mechanosensing via the ECM ligand–integrin–talin–kindlin–F-actin complex. As long as the complex is maintained, a signaling adapter (e.g., paxillin) transduces the occupancy state of the integrin to the interior of the cell. Note that the stability of the complex is allosterically regulated by substrate stiffness, ligand binding affinity, catch bond formation, talin–kindlin affinity for the integrin cytoplasmic peptide, and F-actin–talin interaction. cytopl., cytoplasm; PH, pleckstrin homology; T, talin; K, kindlin.

integrin-, PIPKI-γ–, and layilin-derived peptides (Fig. 8 A), the proposition of a spreading-competent integrin peptide configuration should be possible. Structures of the high-affinity talin-binding peptides of PIPKI-γ (WVY^{p}SPLHYSA; Barsukov et al., 2003; de Pereda et al., 2005; Kong et al., 2006; Wegener et al., 2007) as well as of layilin (WVENEIYY; Wegener et al., 2008) have confirmed the role of W^{739} (W^{775} in β1 integrin) to bind to a hydrophobic pocket created by talin R^{358} (R^{361} in talin2; García-Alvarez et al., 2003; Anthis et al., 2009). Moreover, in these high-affinity structures, the W-V-E/Y^{p}-S/N-P/E-L/I peptide forms a hydrophobic clamp (underlined) stabilized by electrostatic interactions between E/Y^{p} and K^{357}/R^{358} of talin (Fig. 8 A). On the one hand, this high-affinity binding motif enables talin binding in the absence of Y^{747}, while on the other hand, precisely positioning Y^{747} into a shallow hydrophobic pocket, a conformation that is also adopted for binding of β1D to talin2 (Fig. 8 A; Anthis et al., 2009). Interestingly, this shallow binding of Y^{747} creates a hydrophobic surface, potentially enabling interactions with

signaling adapters, such as paxillin (Fig. 8 B). For this site to be accessible, however, the integrin peptide needs to be in a flattened conformation. This is prevented in the PIPKI-γ–derived peptide (β3-SPLH chimera), as a result of looping of the integrin-bound peptide (Wegener et al., 2007), and thereby potentially obstructing access for signaling adapters. Such a scenario would explain the lack of spreading by the β3-SPLH chimera as well as the critical role of kindlin in binding the C-terminal integrin peptide to allow unrestricted access of a signaling adapter to the talin-bound NPLY peptide (Moser et al., 2008; Harburger et al., 2009; Bledzka et al., 2012; Yates et al., 2012). Consistent with this model, the $S^{752}P$ (but not $S^{752}A$; Kieffer et al., 1996) mutation would change the β3 peptide into a conformation no longer compatible with kindlin binding (Ma et al., 2008) and adapter recruitment, such as paxillin. Thus, we propose that talin and kindlin share their triple role in (a) integrin activation (Ma et al., 2008) and (b) integrin clustering (Cluzel et al., 2005; Schmidt et al., 2011) as well as (c) integrin signaling.

To conclude, we propose a model in which integrin, talin, and kindlin form an extracellular ligand-bound protein complex, to which signaling adapter proteins such as paxillin and FAK are recruited once the $NPLY^{747}$ peptide is presented and exposed in a talin-bound and kindlin-regulated conformation (Fig. 8 C). Such a mechanism would restrict mechanosensing to cellular sites where integrins are bound to their ECM ligands, while creating a signaling hub that can integrate different intracellular signaling pathways via the posttranslational modifications of signaling adapter proteins, such as paxillin. This particular organization of focal adhesions would allow independent experimental and therapeutic intervention at the level of cell–matrix binding as well as intracellular signaling.

Materials and methods

cDNAs and site-directed mutagenesis

cDNA encoding full-length mouse β3-GFP-integrin fusion protein expressed in a cytomegalovirus promoter–driven pcDNA3/EGFP vector has been previously described (Ballestrem et al., 2001). Integrin point mutations were introduced by primer overlap extension and verified by automated sequencing.

The β3-SPLH chimera with the high-affinity, talin-binding sequence from PIPK1-γ was constructed by replacing the β3-$NPLY^{747}$ motif with residues from the C terminus of PIPK1-γ (Wegener et al., 2007): K^{738}WDTANNPLY^{747}KEAT (β3 integrin) to K^{738}WVYSPLH^{745}YSAT (β3 chimera; modified residues underlined; Saltel et al., 2009). The β3-VE talin-binding, high-affinity chimera was obtained by replacing the D^{740}TAN sequence of β3 integrin with the VE sequence from the layilin protein: K^{738}WDTANNPLY^{747}KEAT (β3 integrin) to K^{738}WVENPLY^{745}KEAT (β3-VE chimera).

Full-length mouse N-terminal EGFP-tagged talin1 was obtained from A. Huttenlocher (University of Wisconsin School of Medicine, Madison, WI). A red fluorescent version was generated by exchanging EGFP with mRFP (talin1-mRFP) and expressed in a pcDNA3 vector under the cytomegalovirus promoter control. GST–talin head (1–435 aa) and GST–β3-tail (716–762 aa) fusion constructs used for pull-down and Octet biosensor experiments were obtained after cloning of PCR-amplified fragments of human talin1 and mouse β3 integrin into pGex-2T at BamHI–EcoRI sites as previously described (Saltel et al., 2009). Empty pGex-2T vector was used to produce GST for control experiments. His-tagged human talin head was generated by inserting residues 1–406 of human talin1 into the pTrcHisC vector at the BamHI site. DNA sequence analysis was performed for all constructs to ensure error-free amplification and proper base replacement.

Cell culture and transient transfection

NIH-3T3 fibroblasts and COS-7 cells were grown at 37°C (10% CO_2) in DMEM supplemented with 10% FCS, antibiotics (penicillin-streptomycin), and glutamine. Transient transfection was performed with jetPEI (Polyplus Transfection) according to the manufacturer's recommendations. After 6 h, in the jetPEI-containing transfection mix, cells were cultured in complete culture medium for 48 h before detachment for spreading experiments.

Spreading analysis

48 h after transfection, NIH-3T3 fibroblasts were detached with trypsin-EDTA solution and washed once with complete medium containing 10% FCS and twice with PBS to remove phenol red and FCS before FACS sorting. Cells were sorted and selected for their expression of β3-GFP-integrin fluorescence. Cells transfected with nontagged mouse β3 integrin were labeled with a hamster mAb anti–mouse β3 integrin (clone 2C9.G2; BD) and R-phycoerythrin–conjugated goat anti–hamster IgG (Jackson ImmunoResearch Laboratories, Inc.). Sorted cells were washed two times with serum-free medium, resuspended, and plated on previously coated glass coverslips in serum-free DMEM medium containing 0.5% of human serum albumin (HSA; Sigma-Aldrich). Glass coverslips were coated during 1 h at room temperature with purified human VN or FN (Sigma-Aldrich; initially obtained from S. Kanse, University of Oslo, Oslo, Norway [VN] and M. Chiquet, University of Bern, Bern, Switzerland [FN]) diluted in PBS at the indicated concentrations (1 µg/ml VN and 10 µg/ml FN) followed by PBS washing and blocking with 5 mg/ml HSA diluted in PBS.

Spreading curves were obtained from phase-contrast images of living cells maintained at 37°C in a humidified chamber at 15, 30, 60, 120, 240, and 360 min. Spreading was quantified from 10 randomly chosen fields, taken by a 10× long-distance objective on a camera-equipped microscope (Axiovert 100M; Carl Zeiss) using the MetaMorph imaging software (Molecular Devices). Spreading was defined according to morphological criteria: nonspread cells were identified by their round and bright phase-contrast appearance, whereas spreading cells were of dark phase-contrast appearance, exhibiting either a peripheral lamellipodia (fried egg shape) or mechanically stable projections. The spreading curves obtained for the different β3-expressing cells correspond to the mean of at least three independent experiments, and error bars represent the standard error.

Visualization of CMAs by TIRF imaging

Cells were plated for 1 or 6 h on VN- or FN-coated glass coverslips and fixed using 4% PFA in PBS and stored and visualized by TIRF imaging in PBS. TIRF microscopy was performed at room temperature on a microscope (Axiovert 100M) equipped with a combined epifluorescence/TIRF adapter (TILL Photonics), a 100×, NA 1.45 objective (Carl Zeiss), and a 12-bit charge-coupled device camera (Orca ER-9742-95; Hamamatsu Photonics). GFP was excited with the 488-nm line of an adjustable 50-mW diode laser (Sapphire 488–50; Coherent, Inc.), and red dyes were excited with the 535-nm line of a 20-mW diode laser (Compass 215M-20; Coherent, Inc.). Background and contrast were adjusted using the Levels command in Photoshop (Adobe).

Flow cytometry and integrin activation analysis

48 h after transfection, NIH-3T3 fibroblasts were trypsinized and washed once with complete medium and twice with PBS. Cells were stained for endogenous cell surface–exposed β1 integrins with rat mAb 9EG7, recognizing an epitope in ligand-bound integrins, and hamster mAb HMβ1-1, detecting all conformations of β1 integrins. Total cell surface or activated αvβ3 integrins were detected using a hamster anti–mouse β3 integrin mAb (2C9.G2; BD) or the RGD-containing Kistrin-CD31 fusion protein (SKI-7), respectively, followed by a rat anti-CD31 mAb (GC-51; Ballestrem et al., 2001). Hamster and rat mAbs were detected with R-phycoerythrin–conjugated goat anti–hamster IgG or goat anti–rat IgG (SouthernBiotech), respectively. Incubation time was 30 min at 4°C, and for each sample, 10^4 events were acquired on a flow cytometer (Accuri C6; Accuri Cytometers, Inc.) and analyzed with the Accuri C6 software. For each β3 construct, the geometric mean of SKI-7 staining (activated αvβ3 integrin) was divided by the geometric mean of anti-β3 staining (revealing total β3 surface expression), to obtain the relative expression of activated β3 integrins at the cell surface. The activation index was obtained after normalization to wild-type β3-GFP-integrin–transfected cells. Results represent standard error and the mean of at least three independent experiments.

Western blotting and GST pull-down

COS-7 cells transiently transfected with wild-type or mutant β3-GFP-integrin were incubated with lysis buffer (120 mM NaCl, 50 mM Tris-HCl, pH 8.0, 1% Nonidet P-40, 0.5% deoxycholate, 0.1% SDS, 1 mM PMSF, and 1 µg/ml chymostatin, leupeptin, antipain, and pepstatin; all obtained from Sigma-Aldrich) during 5 min on ice. After centrifugation, cell lysates were precleared

with noncoupled glutathione–Sepharose 4B beads (GE Healthcare) at 4°C for 1 h. Precleared lysates where then incubated at 4°C for 1 h with GST- or GST–talin head-loaded glutathione beads, obtained by incubation with bacterial lysates according to standard protocols. After incubation, beads were washed three times with lysis buffer and boiled in standard reducing SDS-PAGE sample buffer. SDS-PAGE and Western blotting were performed according to standard protocols. GFP-tagged proteins were detected with mouse anti-EGFP mAb (Covance) and revealed by anti–mouse HRP-coupled antibody (Jackson ImmunoResearch Laboratories, Inc.).

Recombinant protein purification

Expression of GST-β3-tail chimeras and GST control protein in *Escherichia coli* BL21 Star cells (Invitrogen) was induced by 1 mM IPTG for 5 h at 37°C, after which the collected cells were lysed by homogenization (EmulsiFlex C3; Avestin, Inc.) into PBS. After clarification by centrifugation, lysates were incubated in glutathione–Sepharose (4 Fast Flow; GE Healthcare) suspension overnight. After washing with PBS, proteins were eluted using 50 mM Tris-HCl and 20 mM reduced glutathione, pH 8, and dialyzed into 50 mM sodium phosphate buffer (150 mM NaCl, pH 7.2) before analysis by SDS-PAGE, Coomassie blue staining, and concentration determination by UV/visible spectrometry (A280).

His_6-tagged talin head domain (residues 1–406) was produced in BL21 Star cells as described in the previous paragraph for GST-integrins. Cells were lysed in 20 mM sodium phosphate buffer (1 M NaCl and 20 mM imidazole, pH 7.4). After clarification by centrifugation, lysates were loaded into affinity columns (HisTrap FF; GE Healthcare) using a liquid chromatography system (ÄKTA Purifier; GE Healthcare), washed, and eluted with a linear imidazole gradient 0–700 mM. Eluted fractions were further purified by cation exchange chromatography using HiTrap SP FF columns (GE Healthcare), by loading pooled peak fractions diluted 1:10 in 20 mM Tris-HCl and 20 mM NaCl, pH 7.5. The bound proteins were eluted with a linear NaCl gradient in the loading buffer. Elution of talin head was observed at ∼550 mM NaCl. Eluted fractions were concentrated by a 30-kD filter, analyzed by SDS-PAGE and Coomassie blue staining and estimated to be >95% pure.

Octet biosensor analysis

Biosensor analysis was performed on a Fortebio Octet RED384 instrument (Pall Life Sciences) using a Ni–nitrilotriacetic acid (NTA) sensor chip. A temperature of 25°C and a stirring speed of 1,000 rpm were used throughout the experiment. Sensors were chemically activated by immersing them in 0.1 M EDC and 0.05 M *N*-hydroxysuccinimide (NHS; Thermo Fisher Scientific) in H_2O for 100 s. 50 µg/ml His–talin head was applied in 50 mM $NaPO_3$ and 150 mM NaCl, pH 7.2, resulting in a binding response of ∼8 nm after 300 s. The remaining activated groups were then quenched by 1 M ethanolamine, pH 8.5, for 100 s. Control experiments were performed without cross-linker, demonstrating identical results, requiring, however, more extensive baseline corrections as a result of leakage of talin head from the Ni-NTA.

To obtain relative affinities of different GST-β3-tail chimeras for talin head, serially diluted GST fusion proteins were applied on the talin-coated sensors in concentrations of 20–1,250 nM. GST binding to the sensor was measured for 300 s before applying the next higher protein concentration.

Microcontact printing of patterned substrates

Masters and stamps for microcontact printing were produced as previously described (Lehnert et al., 2004). In brief, masters were fabricated from silicon wafers by low-voltage electron beam lithography using a positive tone. The resulting resist pattern was inverted using a lift-off process and reactive ion etching to yield a master with rectangular, 650-nm-deep holes in the silicon surface. Silicone stamps were produced by the thin stamp technique using Sylgard 184 (Corning).

Stamps were incubated with nine parts unlabeled human FN at 5 µg/ml and one part Alexa Fluor 647–labeled bovine FN (protein-labeling kit; Life Technologies) for 10 min. After drying under nitrogen, stamps were pressed onto glass coverslip for 10 min. Protein-free regions were coated by incubation with 5 µg/ml human VN (Sigma-Aldrich) for 1 h. Coverslips were rinsed once with PBS before seeding and culturing of transiently transfected NIH-3T3 cells in DMEM containing 10% FCS. After 4 h, cells were fixed and stained with antipaxillin as described in the following paragraphs.

Structured illumination microscopy (SIM)

SIM was performed at room temperature with a Plan Apochromat 63×, 1.40 NA oil differential interference contrast objective (Carl Zeiss) on a nonserial prototype (ELYRA PS.1; Carl Zeiss) in superresolution SIM mode, comparable to a commercial PS.1 microscope.

PAA gel cell culture substrates

Thin PAA gel cell culture substrates were made according to published protocols (Buxboim et al., 2010). Cleaned and dried glass coverslips were aminosilanized under vacuum for 1 h with (3-aminopropyl)-triethoxysilane (Sigma-Aldrich). Coverslips were then activated with 0.5% glutaraldehyde (in PBS) for 30 min followed by extensive washing with H_2O. Degassed acrylamide/bisacrylamide mixtures were prepared in 50 mM Hepes-buffered solution to obtain soft (5/0.025%; ∼1.5 kPa) and stiff gels (8/0.1%; ∼30 kPa; Yeung et al., 2005; Tse and Engler, 2010) and mixed with ammonium persulfate and tetramethylethylenediamine (Sigma-Aldrich) to final concentrations of 0.06% wt/vol and 0.4% vol/vol, respectively. Mixtures were immediately added onto the glutaraldehyde-activated coverslips, covered with a cleaned, nontreated glass coverslip, and left to polymerize to obtain a gel of ∼50-µm thickness. After polymerization, coverslip removal, and rinsing, gel surfaces were incubated with the cross-linker Sulfo-SANPAH (Thermo Fisher Scientific; 1 mg/ml in 50 mM Hepes; 80 µl per coverslip). The cross-linker–coated gels were photoactivated by exposure to UV for 2 × 1.5 min, quickly rinsed, and then incubated with a 1-mg/ml FN (YO Proteins) solution for 1 h at 37°C.

To compensate for lower FN cross-linking with UV-induced activation on soft PAA gels, we also used an alternative FN cross-linking strategy (Rajagopalan et al., 2004) that provided similar results (Fig. S4). During the polymerization of the PAA gels, 59 µM NHS acrylic acid was included into acrylamide/bisacrylamide mixture. FN was cross-linked by covering the polymerization mixtures with coverslips first coated with 30 mg/ml BSA and subsequently with 250 µg/ml FN. During polymerization, the acrylic acid NHS incorporated into the PAA gel and simultaneously cross-linked the FN onto the surface of the gel. For both procedures, gels were washed in PBS and conditioned for 1 h before the addition of cells in HSA-containing DMEM.

Immunostaining of fixed cells

Transiently transfected cells were plated for the indicated time on specific substrates (VN- or FN-coated glass or FN-coated PAA gels), fixed with 4% PFA/PBS, and washed with PBS. Cells were blocked and permeabilized for 30 min with a solution of PBS containing 1% BSA and 0.2% Triton X-100. The primary antibody was diluted, applied in PBS containing 1% BSA, and incubated for 30 min followed by three washes, and the incubation was subjected for 30 min with the secondary antibody in the same buffer. Finally cells were washed, imaged, and stored in PBS.

The following antibodies were used for the different experiments: mouse mAb anti–chicken paxillin (clone 349; BD; reacting with mouse paxillin), rat mAb anti–mouse β1 integrin (clone 9EG7; BD), mouse IgM anti-VN (Sigma-Aldrich), mouse mAb antivinculin (V9131; Sigma-Aldrich), rabbit polyclonal antibody to FN (1801; gift from M. Chiquet, University of Bern, Bern, Switzerland), DyLight 549–conjugated goat anti–mouse (Jackson ImmunoResearch Laboratories, Inc.), Cy3-conjugated goat anti–mouse (BD), Cy3-conjugated goat anti–mouse IgM (Dianova), Texas red–conjugated goat anti–rabbit (Jackson ImmunoResearch Laboratories, Inc.), and Texas red–conjugated goat anti–rat (Jackson ImmunoResearch Laboratories, Inc.). F-actin staining was performed using an Alexa Fluor 546–conjugated phalloidin (Molecular Probes).

Epifluorescence images of stained cells were taken in PBS at room temperature, using a 63×, NA 1.4 oil immersion objective on a microscope (Axiovert 100M) equipped with a 10-bit charge-coupled device camera (Orca 9742–95; Hamamatsu Photonics) and the Openlab software (PerkinElmer). Cells grown on PAA gels were mounted in Vectashield and visualized with an microscope (AxioImager ApoTome; Carl Zeiss) equipped with a camera (AxioCam MRm; Carl Zeiss) using a 63×, NA 1.25 or 40×, NA 1.3 Plan Neofluar oil immersion objective (Carl Zeiss).

Antipaxillin colocalization analysis

TIRF images of β3-GFP-integrin and antipaxillin DyLight 549 fluorescence were acquired sequentially. Before colocalization analysis and when required, images were aligned using the RGD alignment plugin in Fiji (National Institutes of Health; Schindelin et al., 2012). Then, a mask was created to analyze only the peripheral areas of the cells containing lamellipodial and filopodial extensions. Using this mask, the Fiji colocalization threshold plugin was used to calculate the Mander's colocalization coefficient with automatic threshold to determine the degree of GFP fluorescence at sites of paxillin staining. A box and whisker plot was drawn using Prism (GraphPad Software) to represent the distribution of the obtained data (n = 30–50 cells per condition), which was however biased to maximal colocalization in cells expressing high levels of integrins. This was particularly relevant for the β3-GFP-SPLH chimera at 4 h, at which relatively large numbers of high-expressing cells were present (Fig. 6 E).

Online supplemental material

Fig. S1 illustrates the low endogenous expression of β3 integrin receptors in the NIH-3T3 cell line used in this work as well as the expression levels of endogenous β1 integrins, after transfection with high-affinity talin-binding β3 integrin mutants. Fig. S2 shows the spreading kinetics of cells transfected with various β3-GFP-integrin mutations and control constructs. Fig. S3 shows the entire blot of the pull-down experiment presented in Fig. 3 D. Fig. S4 illustrates the cell-spreading phenotype and the differential recruitment of wild-type and mutant β3-GFP-integrins into CMAs on stiff versus flexible FN-coated surfaces. Online supplemental material is available at http://www.jcb.org/cgi/content/full/jcb.201308136/DC1. Additional data are available in the JCB DataViewer at http://dx.doi.org/10.1083/jcb.201308136.dv.

The authors thank Drs. Matthias Chiquet, Sandip Kanse, and Anna Huttenlocher for reagents and plasmids, David Boettiger for discussions, and Stuart Prince and Chloe Thomson for reading the manuscript. The Bioimaging Core Facility at the Centre Médical Universitaire, Geneva, Outi Väätäinen, and Ulla Kiiskinen are acknowledged for technical assistance as well as Teemu Ihalainen and Chloe Thomson for help with the PAA gels.

This work was supported by research grants from Nevus Outreach, the Swiss National Science foundation (31003A-130742), and the Swiss Foundation for Research on Myopathies to B. Wehrle-Haller, from the Karlsruhe School of Optics and Photonics to M. Bachmann, and by the Academy of Finland and Sigrid Jusélius Foundation to V.P. Hytönen. This study was financially supported partly by the Competitive State Research Financing of the Expert Responsibility Area of Tampere University Hospital to V.P. Hytönen. Biocenter Finland is acknowledged for financing a short term laboratory visit of P. Pinon to BioMediTech. B. Wehrle-Haller and M. Bastmeyer are members of the COST Action BM1001 (ECMNET).

The authors declare no competing financial interests.

Submitted: 23 August 2013
Accepted: 18 March 2014

References

Akiyama, S.K., S.S. Yamada, K.M. Yamada, and S.E. LaFlamme. 1994. Transmembrane signal transduction by integrin cytoplasmic domains expressed in single-subunit chimeras. *J. Biol. Chem.* 269:15961–15964.

Anthis, N.J., K.L. Wegener, F. Ye, C. Kim, B.T. Goult, E.D. Lowe, I. Vakonakis, N. Bate, D.R. Critchley, M.H. Ginsberg, and I.D. Campbell. 2009. The structure of an integrin/talin complex reveals the basis of inside-out signal transduction. *EMBO J.* 28:3623–3632. http://dx.doi.org/10.1038/emboj.2009.287

Anthis, N.J., K.L. Wegener, D.R. Critchley, and I.D. Campbell. 2010. Structural diversity in integrin/talin interactions. *Structure*. 18:1654–1666. http://dx.doi.org/10.1016/j.str.2010.09.018

Ballestrem, C., B. Hinz, B.A. Imhof, and B. Wehrle-Haller. 2001. Marching at the front and dragging behind: differential αVβ3-integrin turnover regulates focal adhesion behavior. *J. Cell Biol.* 155:1319–1332. http://dx.doi.org/10.1083/jcb.200107107

Barsukov, I.L., A. Prescot, N. Bate, B. Patel, D.N. Floyd, N. Bhanji, C.R. Bagshaw, K. Letinic, G. Di Paolo, P. De Camilli, et al. 2003. Phosphatidylinositol phosphate kinase type 1gamma and beta1-integrin cytoplasmic domain bind to the same region in the talin FERM domain. *J. Biol. Chem.* 278:31202–31209. http://dx.doi.org/10.1074/jbc.M303850200

Berrier, A.L., A.M. Mastrangelo, J. Downward, M. Ginsberg, and S.E. LaFlamme. 2000. Activated R-ras, Rac1, PI 3-kinase and PKCε can each restore cell spreading inhibited by isolated integrin β1 cytoplasmic domains. *J. Cell Biol.* 151:1549–1560. http://dx.doi.org/10.1083/jcb.151.7.1549

Berrier, A.L., R. Martinez, G.M. Bokoch, and S.E. LaFlamme. 2002. The integrin beta tail is required and sufficient to regulate adhesion signaling to Rac1. *J. Cell Sci.* 115:4285–4291. http://dx.doi.org/10.1242/jcs.00109

Bledzka, K., J. Liu, Z. Xu, H.D. Perera, S.P. Yadav, K. Bialkowska, J. Qin, Y.Q. Ma, and E.F. Plow. 2012. Spatial coordination of kindlin-2 with talin head domain in interaction with integrin β cytoplasmic tails. *J. Biol. Chem.* 287:24585–24594. http://dx.doi.org/10.1074/jbc.M111.336743

Boettiger, D. 2012. Mechanical control of integrin-mediated adhesion and signaling. *Curr. Opin. Cell Biol.* 24:592–599. http://dx.doi.org/10.1016/j.ceb.2012.07.002

Brown, M.C., J.A. Perrotta, and C.E. Turner. 1996. Identification of LIM3 as the principal determinant of paxillin focal adhesion localization and characterization of a novel motif on paxillin directing vinculin and focal adhesion kinase binding. *J. Cell Biol.* 135:1109–1123. http://dx.doi.org/10.1083/jcb.135.4.1109

Bunch, T.A. 2010. Integrin alphaIIbbeta3 activation in Chinese hamster ovary cells and platelets increases clustering rather than affinity. *J. Biol. Chem.* 285:1841–1849. http://dx.doi.org/10.1074/jbc.M109.057349

Buxboim, A., K. Rajagopal, A.E. Brown, and D.E. Discher. 2010. How deeply cells feel: methods for thin gels. *J. Phys. Condens. Matter*. 22:194116. http://dx.doi.org/10.1088/0953-8984/22/19/194116

Chen, Y.P., T.E. O'Toole, J. Ylänne, J.P. Rosa, and M.H. Ginsberg. 1994. A point mutation in the integrin beta 3 cytoplasmic domain (S752—>P) impairs bidirectional signaling through alpha IIb beta 3 (platelet glycoprotein IIb-IIIa). *Blood*. 84:1857–1865.

Choi, C.H., B.A. Webb, M.S. Chimenti, M.P. Jacobson, and D.L. Barber. 2013. pH sensing by FAK-His58 regulates focal adhesion remodeling. *J. Cell Biol.* 202:849–859. http://dx.doi.org/10.1083/jcb.201302131

Choi, C.K., J. Zareno, M.A. Digman, E. Gratton, and A.R. Horwitz. 2011. Cross-correlated fluctuation analysis reveals phosphorylation-regulated paxillin-FAK complexes in nascent adhesions. *Biophys. J.* 100:583–592. http://dx.doi.org/10.1016/j.bpj.2010.12.3719

Cluzel, C., F. Saltel, J. Lussi, F. Paulhe, B.A. Imhof, and B. Wehrle-Haller. 2005. The mechanisms and dynamics of αvβ3 integrin clustering in living cells. *J. Cell Biol.* 171:383–392. http://dx.doi.org/10.1083/jcb.200503017

Deakin, N.O., and C.E. Turner. 2008. Paxillin comes of age. *J. Cell Sci.* 121:2435–2444. http://dx.doi.org/10.1242/jcs.018044

Deakin, N.O., and C.E. Turner. 2011. Distinct roles for paxillin and Hic-5 in regulating breast cancer cell morphology, invasion, and metastasis. *Mol. Biol. Cell*. 22:327–341. http://dx.doi.org/10.1091/mbc.E10-09-0790

del Rio, A., R. Perez-Jimenez, R. Liu, P. Roca-Cusachs, J.M. Fernandez, and M.P. Sheetz. 2009. Stretching single talin rod molecules activates vinculin binding. *Science*. 323:638–641. http://dx.doi.org/10.1126/science.1162912

de Pereda, J.M., K.L. Wegener, E. Santelli, N. Bate, M.H. Ginsberg, D.R. Critchley, I.D. Campbell, and R.C. Liddington. 2005. Structural basis for phosphatidylinositol phosphate kinase type Igamma binding to talin at focal adhesions. *J. Biol. Chem.* 280:8381–8386. http://dx.doi.org/10.1074/jbc.M413180200

Engler, A.J., S. Sen, H.L. Sweeney, and D.E. Discher. 2006. Matrix elasticity directs stem cell lineage specification. *Cell*. 126:677–689. http://dx.doi.org/10.1016/j.cell.2006.06.044

Friedland, J.C., M.H. Lee, and D. Boettiger. 2009. Mechanically activated integrin switch controls alpha5beta1 function. *Science*. 323:642–644. http://dx.doi.org/10.1126/science.1168441

García-Alvarez, B., J.M. de Pereda, D.A. Calderwood, T.S. Ulmer, D. Critchley, I.D. Campbell, M.H. Ginsberg, and R.C. Liddington. 2003. Structural determinants of integrin recognition by talin. *Mol. Cell*. 11:49–58. http://dx.doi.org/10.1016/S1097-2765(02)00823-7

Gingras, A.R., W.H. Ziegler, R. Frank, I.L. Barsukov, G.C. Roberts, D.R. Critchley, and J. Emsley. 2005. Mapping and consensus sequence identification for multiple vinculin binding sites within the talin rod. *J. Biol. Chem.* 280:37217–37224. http://dx.doi.org/10.1074/jbc.M508060200

Goksoy, E., Y.Q. Ma, X. Wang, X. Kong, D. Perera, E.F. Plow, and J. Qin. 2008. Structural basis for the autoinhibition of talin in regulating integrin activation. *Mol. Cell*. 31:124–133. http://dx.doi.org/10.1016/j.molcel.2008.06.011

Green, J.A., A.L. Berrier, R. Pankov, and K.M. Yamada. 2009. beta1 integrin cytoplasmic domain residues selectively modulate fibronectin matrix assembly and cell spreading through talin and Akt-1. *J. Biol. Chem.* 284:8148–8159. http://dx.doi.org/10.1074/jbc.M805934200

Guillou, H., A. Depraz-Depland, E. Planus, B. Vianay, J. Chaussy, A. Grichine, C. Albigès-Rizo, and M.R. Block. 2008. Lamellipodia nucleation by filopodia depends on integrin occupancy and downstream Rac1 signaling. *Exp. Cell Res.* 314:478–488. http://dx.doi.org/10.1016/j.yexcr.2007.10.026

Hagel, M., E.L. George, A. Kim, R. Tamimi, S.L. Opitz, C.E. Turner, A. Imamoto, and S.M. Thomas. 2002. The adaptor protein paxillin is essential for normal development in the mouse and is a critical transducer of fibronectin signaling. *Mol. Cell. Biol.* 22:901–915. http://dx.doi.org/10.1128/MCB.22.3.901-915.2002

Harburger, D.S., M. Bouaouina, and D.A. Calderwood. 2009. Kindlin-1 and -2 directly bind the C-terminal region of beta integrin cytoplasmic tails and exert integrin-specific activation effects. *J. Biol. Chem.* 284:11485–11497. http://dx.doi.org/10.1074/jbc.M809233200

Hynes, R.O. 2002. Integrins: bidirectional, allosteric signaling machines. *Cell*. 110:673–687. http://dx.doi.org/10.1016/S0092-8674(02)00971-6

Hytönen, V.P., and V. Vogel. 2008. How force might activate talin's vinculin binding sites: SMD reveals a structural mechanism. *PLOS Comput. Biol.* 4:e24. http://dx.doi.org/10.1371/journal.pcbi.0040024

Kieffer, N., C. Melchior, J.M. Guinet, S. Michels, V. Gouon, and N. Bron. 1996. Serine 752 in the cytoplasmic domain of the beta 3 integrin subunit is

not required for alpha v beta 3 postreceptor signaling events. *Cell Adhes. Commun.* 4:25–39. http://dx.doi.org/10.3109/15419069609010761

Kong, F., A.J. García, A.P. Mould, M.J. Humphries, and C. Zhu. 2009. Demonstration of catch bonds between an integrin and its ligand. *J. Cell Biol.* 185:1275–1284. http://dx.doi.org/10.1083/jcb.200810002

Kong, X., X. Wang, S. Misra, and J. Qin. 2006. Structural basis for the phosphorylation-regulated focal adhesion targeting of type Igamma phosphatidylinositol phosphate kinase (PIPKIgamma) by talin. *J. Mol. Biol.* 359:47–54. http://dx.doi.org/10.1016/j.jmb.2006.02.048

LaFlamme, S.E., L.A. Thomas, S.S. Yamada, and K.M. Yamada. 1994. Single subunit chimeric integrins as mimics and inhibitors of endogenous integrin functions in receptor localization, cell spreading and migration, and matrix assembly. *J. Cell Biol.* 126:1287–1298. http://dx.doi.org/10.1083/jcb.126.5.1287

Lawson, C., S.T. Lim, S. Uryu, X.L. Chen, D.A. Calderwood, and D.D. Schlaepfer. 2012. FAK promotes recruitment of talin to nascent adhesions to control cell motility. *J. Cell Biol.* 196:223–232. http://dx.doi.org/10.1083/jcb.201108078

Lehnert, D., B. Wehrle-Haller, C. David, U. Weiland, C. Ballestrem, B.A. Imhof, and M. Bastmeyer. 2004. Cell behaviour on micropatterned substrata: limits of extracellular matrix geometry for spreading and adhesion. *J. Cell Sci.* 117:41–52. http://dx.doi.org/10.1242/jcs.00836

Ma, Y.Q., J. Qin, C. Wu, and E.F. Plow. 2008. Kindlin-2 (Mig-2): a co-activator of β_3 integrins. *J. Cell Biol.* 181:439–446. http://dx.doi.org/10.1083/jcb.200710196

Miyamoto, S., S.K. Akiyama, and K.M. Yamada. 1995. Synergistic roles for receptor occupancy and aggregation in integrin transmembrane function. *Science*. 267:883–885. http://dx.doi.org/10.1126/science.7846531

Miyamoto, S., H. Teramoto, J.S. Gutkind, and K.M. Yamada. 1996. Integrins can collaborate with growth factors for phosphorylation of receptor tyrosine kinases and MAP kinase activation: roles of integrin aggregation and occupancy of receptors. *J. Cell Biol.* 135:1633–1642. http://dx.doi.org/10.1083/jcb.135.6.1633

Monkley, S.J., X.-H. Zhou, S.J. Kinston, S.M. Giblett, L. Hemmings, H. Priddle, J.E. Brown, C.A. Pritchard, D.R. Critchley, and R. Fässler. 2000. Disruption of the talin gene arrests mouse development at the gastrulation stage. *Dev. Dyn.* 219:560–574. http://dx.doi.org/10.1002/1097-0177(2000)9999:9999<::AID-DVDY1079>3.0.CO;2-Y

Monkley, S.J., V. Kostourou, L. Spence, B. Petrich, S. Coleman, M.H. Ginsberg, C.A. Pritchard, and D.R. Critchley. 2011. Endothelial cell talin1 is essential for embryonic angiogenesis. *Dev. Biol.* 349:494–502. http://dx.doi.org/10.1016/j.ydbio.2010.11.010

Montanez, E., S. Ussar, M. Schifferer, M. Bösl, R. Zent, M. Moser, and R. Fässler. 2008. Kindlin-2 controls bidirectional signaling of integrins. *Genes Dev.* 22:1325–1330. http://dx.doi.org/10.1101/gad.469408

Moser, M., B. Nieswandt, S. Ussar, M. Pozgajova, and R. Fässler. 2008. Kindlin-3 is essential for integrin activation and platelet aggregation. *Nat. Med.* 14:325–330. http://dx.doi.org/10.1038/nm1722

Moser, M., M. Bauer, S. Schmid, R. Ruppert, S. Schmidt, M. Sixt, H.V. Wang, M. Sperandio, and R. Fässler. 2009. Kindlin-3 is required for beta2 integrin-mediated leukocyte adhesion to endothelial cells. *Nat. Med.* 15:300–305. http://dx.doi.org/10.1038/nm.1921

Partridge, M.A., and E.E. Marcantonio. 2006. Initiation of attachment and generation of mature focal adhesions by integrin-containing filopodia in cell spreading. *Mol. Biol. Cell*. 17:4237–4248. http://dx.doi.org/10.1091/mbc.E06-06-0496

Paszek, M.J., N. Zahir, K.R. Johnson, J.N. Lakins, G.I. Rozenberg, A. Gefen, C.A. Reinhart-King, S.S. Margulies, M. Dembo, D. Boettiger, et al. 2005. Tensional homeostasis and the malignant phenotype. *Cancer Cell*. 8:241–254. http://dx.doi.org/10.1016/j.ccr.2005.08.010

Petrich, B.G., P. Fogelstrand, A.W. Partridge, N. Yousefi, A.J. Ablooglu, S.J. Shattil, and M.H. Ginsberg. 2007a. The antithrombotic potential of selective blockade of talin-dependent integrin alpha IIb beta 3 (platelet GPIIb-IIIa) activation. *J. Clin. Invest.* 117:2250–2259. http://dx.doi.org/10.1172/JCI31024

Petrich, B.G., P. Marchese, Z.M. Ruggeri, S. Spiess, R.A. Weichert, F. Ye, R. Tiedt, R.C. Skoda, S.J. Monkley, D.R. Critchley, and M.H. Ginsberg. 2007b. Talin is required for integrin-mediated platelet function in hemostasis and thrombosis. *J. Exp. Med.* 204:3103–3111. http://dx.doi.org/10.1084/jem.20071800

Pluskota, E., J.J. Dowling, N. Gordon, J.A. Golden, D. Szpak, X.Z. West, C. Nestor, Y.Q. Ma, K. Bialkowska, T. Byzova, and E.F. Plow. 2011. The integrin coactivator kindlin-2 plays a critical role in angiogenesis in mice and zebrafish. *Blood*. 117:4978–4987. http://dx.doi.org/10.1182/blood-2010-11-321182

Rajagopalan, P., W.A. Marganski, X.Q. Brown, and J.Y. Wong. 2004. Direct comparison of the spread area, contractility, and migration of balb/c 3T3 fibroblasts adhered to fibronectin- and RGD-modified substrata. *Biophys. J.* 87:2818–2827. http://dx.doi.org/10.1529/biophysj.103.037218

Roca-Cusachs, P., N.C. Gauthier, A. del Rio, and M.P. Sheetz. 2009. Clustering of alpha(5)beta(1) integrins determines adhesion strength whereas alpha(v)beta(3) and talin enable mechanotransduction. *Proc. Natl. Acad. Sci. USA*. 106:16245–16250. http://dx.doi.org/10.1073/pnas.0902818106

Saltel, F., E. Mortier, V.P. Hytönen, M.C. Jacquier, P. Zimmermann, V. Vogel, W. Liu, and B. Wehrle-Haller. 2009. New PI(4,5)P_2- and membrane proximal integrin–binding motifs in the talin head control β3-integrin clustering. *J. Cell Biol.* 187:715–731. http://dx.doi.org/10.1083/jcb.200908134

Schaffner-Reckinger, E., V. Gouon, C. Melchior, S. Plançon, and N. Kieffer. 1998. Distinct involvement of beta3 integrin cytoplasmic domain tyrosine residues 747 and 759 in integrin-mediated cytoskeletal assembly and phosphotyrosine signaling. *J. Biol. Chem.* 273:12623–12632. http://dx.doi.org/10.1074/jbc.273.20.12623

Schindelin, J., I. Arganda-Carreras, E. Frise, V. Kaynig, M. Longair, T. Pietzsch, S. Preibisch, C. Rueden, S. Saalfeld, B. Schmid, et al. 2012. Fiji: an open-source platform for biological-image analysis. *Nat. Methods*. 9:676–682. http://dx.doi.org/10.1038/nmeth.2019

Schmidt, S., I. Nakchbandi, R. Ruppert, N. Kawelke, M.W. Hess, K. Pfaller, P. Jurdic, R. Fässler, and M. Moser. 2011. Kindlin-3–mediated signaling from multiple integrin classes is required for osteoclast-mediated bone resorption. *J. Cell Biol.* 192:883–897. http://dx.doi.org/10.1083/jcb.201007141

Shi, Q., and D. Boettiger. 2003. A novel mode for integrin-mediated signaling: tethering is required for phosphorylation of FAK Y397. *Mol. Biol. Cell*. 14:4306–4315. http://dx.doi.org/10.1091/mbc.E03-01-0046

Sin, S., F. Bonin, V. Petit, D. Meseure, F. Lallemand, I. Bièche, A. Bellahcène, V. Castronovo, O. de Wever, C. Gespach, et al. 2011. Role of the focal adhesion protein kindlin-1 in breast cancer growth and lung metastasis. *J. Natl. Cancer Inst.* 103:1323–1337. http://dx.doi.org/10.1093/jnci/djr290

Song, X., J. Yang, J. Hirbawi, S. Ye, H.D. Perera, E. Goksoy, P. Dwivedi, E.F. Plow, R. Zhang, and J. Qin. 2012. A novel membrane-dependent on/off switch mechanism of talin FERM domain at sites of cell adhesion. *Cell Res.* 22:1533–1545. http://dx.doi.org/10.1038/cr.2012.97

Taddei, M.L., E. Giannoni, T. Fiaschi, and P. Chiarugi. 2012. Anoikis: an emerging hallmark in health and diseases. *J. Pathol.* 226:380–393. http://dx.doi.org/10.1002/path.3000

Tadokoro, S., S.J. Shattil, K. Eto, V. Tai, R.C. Liddington, J.M. de Pereda, M.H. Ginsberg, and D.A. Calderwood. 2003. Talin binding to integrin beta tails: a final common step in integrin activation. *Science*. 302:103–106. http://dx.doi.org/10.1126/science.1086652

Tanentzapf, G., and N.H. Brown. 2006. An interaction between integrin and the talin FERM domain mediates integrin activation but not linkage to the cytoskeleton. *Nat. Cell Biol.* 8:601–606. http://dx.doi.org/10.1038/ncb1411

Tse, J.R., and A.J. Engler. 2010. Preparation of hydrogel substrates with tunable mechanical properties. *Curr. Protoc. Cell Biol.* Chapter 10:10.16.1–10.16.16.

Wade, R., J. Bohl, and S. Vande Pol. 2002. Paxillin null embryonic stem cells are impaired in cell spreading and tyrosine phosphorylation of focal adhesion kinase. *Oncogene*. 21:96–107. http://dx.doi.org/10.1038/sj.onc.1205013

Wang, P., C. Ballestrem, and C.H. Streuli. 2011. The C terminus of talin links integrins to cell cycle progression. *J. Cell Biol.* 195:499–513. http://dx.doi.org/10.1083/jcb.201104128

Wegener, K.L., A.W. Partridge, J. Han, A.R. Pickford, R.C. Liddington, M.H. Ginsberg, and I.D. Campbell. 2007. Structural basis of integrin activation by talin. *Cell*. 128:171–182. http://dx.doi.org/10.1016/j.cell.2006.10.048

Wegener, K.L., J. Basran, C.R. Bagshaw, I.D. Campbell, G.C. Roberts, D.R. Critchley, and I.L. Barsukov. 2008. Structural basis for the interaction between the cytoplasmic domain of the hyaluronate receptor layilin and the talin F3 subdomain. *J. Mol. Biol.* 382:112–126. http://dx.doi.org/10.1016/j.jmb.2008.06.087

Wehrle-Haller, B. 2012. Structure and function of focal adhesions. *Curr. Opin. Cell Biol.* 24:116–124. http://dx.doi.org/10.1016/j.ceb.2011.11.001

Yates, L.A., A.K. Füzéry, R. Bonet, I.D. Campbell, and R.J. Gilbert. 2012. Biophysical analysis of Kindlin-3 reveals an elongated conformation and maps integrin binding to the membrane-distal β-subunit NPXY motif. *J. Biol. Chem.* 287:37715–37731. http://dx.doi.org/10.1074/jbc.M112.415208

Yeung, T., P.C. Georges, L.A. Flanagan, B. Marg, M. Ortiz, M. Funaki, N. Zahir, W. Ming, V. Weaver, and P.A. Janmey. 2005. Effects of substrate stiffness on cell morphology, cytoskeletal structure, and adhesion. *Cell Motil. Cytoskeleton*. 60:24–34. http://dx.doi.org/10.1002/cm.20041

Ylänne, J., J. Huuskonen, T.E. O'Toole, M.H. Ginsberg, I. Virtanen, and C.G. Gahmberg. 1995. Mutation of the cytoplasmic domain of the integrin beta 3 subunit. Differential effects on cell spreading, recruitment to adhesion plaques, endocytosis, and phagocytosis. *J. Biol. Chem.* 270:9550–9557.

Zhang, X., G. Jiang, Y. Cai, S.J. Monkley, D.R. Critchley, and M.P. Sheetz. 2008. Talin depletion reveals independence of initial cell spreading from integrin activation and traction. *Nat. Cell Biol.* 10:1062–1068. http://dx.doi.org/10.1038/ncb1765

Zhu, J., J. Zhu, and T.A. Springer. 2013. Complete integrin headpiece opening in eight steps. *J. Cell Biol.* 201:1053–1068. http://dx.doi.org/10.1083/jcb.201212037

Zouq, N.K., J.A. Keeble, J. Lindsay, A.J. Valentijn, L. Zhang, D. Mills, C.E. Turner, C.H. Streuli, and A.P. Gilmore. 2009. FAK engages multiple pathways to maintain survival of fibroblasts and epithelia: differential roles for paxillin and p130Cas. *J. Cell Sci.* 122:357–367. http://dx.doi.org/10.1242/jcs.030478